BNL-75494-2006-JA

JOURNAL OF GEOPHYSICAL RESEARCH, VOL. 108, NO. D23, 8656, doi:10.1029/2002JD003361, 2003

Column closure studies of lower tropospheric aerosol and water vapor during ACE-Asia using airborne Sun photometer and airborne in situ and ship-based lidar measurements

B. Schmid,[1] D. A. Hegg,[2] J. Wang,[3,4] D. Bates,[5] J. Redemann,[1] P. B. Russell,[6] J. M. Livingston,[7] H. H. Jonsson,[8] E. J. Welton,[9] J. H. Seinfeld,[3] R. C. Flagan,[3] D. S. Covert,[2] O. Dubovik,[10] and A. Jefferson[11]

Received 26 December 2002; revised 9 April 2003; accepted 21 April 2003; published 19 August 2003.

[1] We assess the consistency (closure) between solar beam attenuation by aerosols and water vapor measured by airborne Sun photometry and derived from airborne in situ and ship-based lidar measurements during the April 2001 Asian Pacific Regional Aerosol Characterization Experiment (ACE-Asia). The airborne data presented here were obtained aboard the Twin Otter aircraft. Comparing aerosol extinction σ_{ep}(550 nm) from four different techniques shows good agreement for the vertical distribution of aerosol layers. However, the level of agreement in absolute magnitude of the derived aerosol extinction varied among the aerosol layers sampled. The σ_{ep}(550 nm) computed from airborne in situ size distribution and composition measurements shows good agreement with airborne Sun photometry in the marine boundary layer but is considerably lower in layers dominated by dust if the particles are assumed to be spherical. The σ_{ep}(550 nm) from airborne in situ scattering and absorption measurements are about ~13% lower than those obtained from airborne Sun photometry during 14 vertical profiles. Combining lidar and the airborne Sun photometer measurements reveals the prevalence of dust layers at altitudes up to 10 km with layer aerosol optical depth (from 3.5 to 10 km altitude) of ~0.1 to 0.2 (500 nm) and extinction-to-backscatter ratios of 59–71 sr (523 nm). The airborne Sun photometer aboard the Twin Otter reveals a relatively dry atmosphere during ACE-Asia with all water vapor columns <1.5 cm and water vapor densities ρ_w < 12 g/m^3. Comparing layer water vapor amounts and ρ_w from the airborne Sun photometer to the same quantities measured with aircraft in situ sensors leads to a high correlation (r^2 = 0.96), but the Sun photometer tends to underestimate ρ_w by 7%. *INDEX TERMS:* 0305 Atmospheric Composition and Structure: Aerosols and particles (0345, 4801); 0360 Atmospheric Composition and Structure: Transmission and scattering of radiation; 0365 Atmospheric Composition and Structure: Troposphere—composition and chemistry; *KEYWORDS:* aerosol extinction, water vapor, aircraft measurements of aerosol, Sun photometer, lidar

Citation: Schmid, B., et al., Column closure studies of lower tropospheric aerosol and water vapor during ACE-Asia using airborne Sun photometer and airborne in situ and ship-based lidar measurements, *J. Geophys. Res.*, *108*(D23), 8656, doi:10.1029/2002JD003361, 2003.

1. Introduction

[2] In spring when storm and frontal activity are at a maximum in Asia, industrial pollution, biomass burning and mineral dust outflows produce a very complex regional aerosol mix. Of particular interest is the impact of the Asian regional aerosol on radiative fluxes at a variety of atmospheric levels (e.g., the surface, the top of the boundary layer, the upper troposphere, the top of the atmosphere). These flux changes, when sustained over sufficient areas

[1]Bay Area Environmental Research Institute, Sonoma, California, USA.
[2]Department of Atmospheric Sciences, University of Washington, Seattle, Washington, USA.
[3]Department of Chemical Engineering, California Institute of Technology, Pasadena, California, USA.
[4]Now at Brookhaven National Laboratory, Upton, New York, USA.
[5]Physics Department, University of Miami, Coral Gables, Florida, USA.
[6]NASA Ames Research Center, Moffett Field, California, USA.
[7]SRI International, Menlo Park, California, USA.
[8]Center for Interdisciplinary Remotely Piloted Aircraft Studies, Marina, California, USA.
[9]Laboratory for Atmospheres, NASA Goddard Space Flight Center, Greenbelt, Maryland, USA.
[10]Goddard Earth Sciences and Technology Center, NASA Goddard Space Flight Center, Greenbelt, Maryland, USA.
[11]Cooperative Institute for Research in the Environmental Sciences, NOAA Climate Monitoring and Diagnostics Laboratory, Boulder, Colorado, USA.

Copyright 2003 by the American Geophysical Union.
0148-0227/03/2002JD003361$09.00

and times, are the radiative forcings that drive climate processes [e.g., *Kaufman et al.*, 2002; *Ramanathan et al.*, 2001]. However, regional forcing can only be assessed with any degree of certainty if the optical properties of the regional aerosol measured with various techniques from various platforms are mutually consistent.

[3] In April 2001, the Asian Pacific Regional Aerosol Characterization Experiment (ACE-Asia) field studies involving multiple aircraft, ships, satellites, and surface sites obtained comprehensive measurements of combined mineral dust, pollutants and other aerosols [*Huebert et al.*, 2003].

[4] In this paper we assess the consistency (closure) between solar beam attenuation by aerosols and water vapor measured by airborne Sun photometry and derived from airborne in situ, and ship-based lidar methods during the ACE-Asia field experiment. The airborne data presented in this study were obtained aboard the Twin Otter aircraft. A companion paper [*Redemann et al.*, 2003] discusses closure results obtained from the C-130 aircraft. Such closure studies have revealed important insights about aerosol sampling and inadvertent modification in such previous aerosol field experiments as the Tropospheric Aerosol Radiative Forcing Observational Experiment, TARFOX [*Hegg et al.*, 1997; *Hartley et al.*, 2000], the 2nd Aerosol Characterization Experiment, ACE-2 [*Collins et al.*, 2000; *Schmid et al.*, 2000], the Indian Ocean Experiment, INDOEX [*Masonis et al.*, 2002] and the Southern African Regional Science Initiative, SAFARI 2000 [*Magi et al.*, 2003].

2. Measurements

2.1. Airborne Measurements

2.1.1. The Twin Otter Aircraft

[5] The Twin Otter is operated by the Marina, California-based Center for Interdisciplinary Remotely Piloted Aircraft Studies (CIRPAS) [*Bluth et al.*, 1996]. The CIRPAS UV-18A Twin Otter is the military version of the DeHavilland DHC-6-300. Between 31 March and 1 May 2001 the Twin Otter performed 19 research flights out of Iwakuni Marine Corps Air Station, near Hiroshima, Japan (34.15°N, 132.23°E, 0 m). For the ACE-Asia campaign the maximum flight altitude was about 3.8 km.

[6] The aircraft position (i.e., geographical latitude and longitude and altitude above sea level) was determined using onboard Global Positioning System (GPS) receivers. In order to have accurate time stamps the Payload Data Management System time was synchronized with GPS time. Sensors aboard the Twin Otter measured static temperature T, static pressure p, and dewpoint temperature T_d. For comparison with the airborne Sun photometer water vapor retrievals, we computed the water vapor density ρ_w as a function of T, p, and T_d using an expression given by *Bögel* [1977].

2.1.2. Aerosol Extinction From Airborne Sun Photometry

[7] The NASA Ames Airborne Tracking 14-channel Sun photometer (AATS-14) measures the transmission of the direct solar beam in 14 spectral channels (354 to 1558 nm). AATS-14 is an enhanced version of the AATS-6 instrument [*Matsumoto et al.*, 1987], which flew on the C-130 aircraft during ACE-Asia [*Redemann et al.*, 2003].

[8] AATS-14 azimuth and elevation motors, controlled by tracking-error signals derived from a quad-cell photodiode, rotate a tracking head to lock on to the solar beam and keep detectors normal to it. The tracking head is mounted outside the aircraft skin to minimize blockage by aircraft structures and to avoid data contamination by aircraft-window effects. Window defogging is achieved by a foil heater. Each channel consists of a baffled entrance path, interference filter, photodiode detector, and integral preamplifier. The filter/detector/preamp sets are temperature controlled to avoid thermally induced calibration changes.

[9] AATS-14 is designed to operate on a variety of aircraft, some of which may be remotely piloted. It can locate and track the sun without input from an operator and record data in a self-contained data system. In addition, it must interface to an aircraft-provided data system, and receive and execute commands from a remote operator station (laptop), and transmit science and instrument-status data to that station. Using aircraft-provided data on latitude, longitude and ambient static pressure, aerosol (or particulate) optical depth $\tau_p(\lambda)$ and columnar water vapor CWV are computed in real-time and displayed at the operator station (along with raw data, instrument status, and aircraft-provided data). Radiometric calibration is determined from Langley plots [*Schmid and Wehrli*, 1995], either at high-mountain observatories or during specially designed flights [*Schmid et al.*, 2000].

[10] AATS-14 made its first science flights on the CIRPAS Pelican (modified Cessna) aircraft during the Tropospheric Aerosol Radiative Forcing Observational Experiment (TARFOX) in July 1996 [*Russell et al.*, 1999a, 1999b]. More extensive flights on the Pelican were made in ACE-2, which provided many measurements of marine, European pollution, and African dust aerosol optical depth spectra, as well as water vapor columns [*Schmid et al.*, 2000]. Operating aboard the University of Washington's Convair-580 research aircraft, AATS-14 provided detailed measurements of African biomass burning aerosol during SAFARI 2000 [*Schmid et al.*, 2003]. In ACE-Asia, AATS-14 operated successfully during all 19 Twin Otter research flights. The tracking head was moved into its park position when flying through or under clouds.

[11] Our methods for data reduction, calibration, and error analysis have been described previously [*Russell et al.*, 1993a; *Schmid and Wehrli*, 1995; *Schmid et al.*, 1998, 2001]. A brief summary is given here. The AATS-14 channels are chosen to allow separation of aerosol, water vapor, and ozone transmission. From these slant-path transmissions we retrieve $\tau_p(\lambda)$ in 13 narrow wavelength bands and the columnar amounts of water vapor and ozone. In addition to the corrections for Rayleigh scattering and O_3 absorption, some channels require corrections for NO_2, H_2O and O_2-O_2 absorption. Cross-sections were computed using LBLRTM 6.01 [*Clough and Iacono*, 1995] with the CKD 2.4.1 continuum model using the HITRAN 2000 (v 11.0) line-list [*Rothman et al.*, 2001; *Rothman and Schroeder*, 2002] (including an update for water vapor from April 2001, see http://www.hitran.com/hitran/updates.html). NO_2 cross-sections not included in LBLRTM 6.01 were taken from *Harder et al.* [1997]. NO_2 was assumed constant at 2×10^{-15} molecules cm^{-2}.

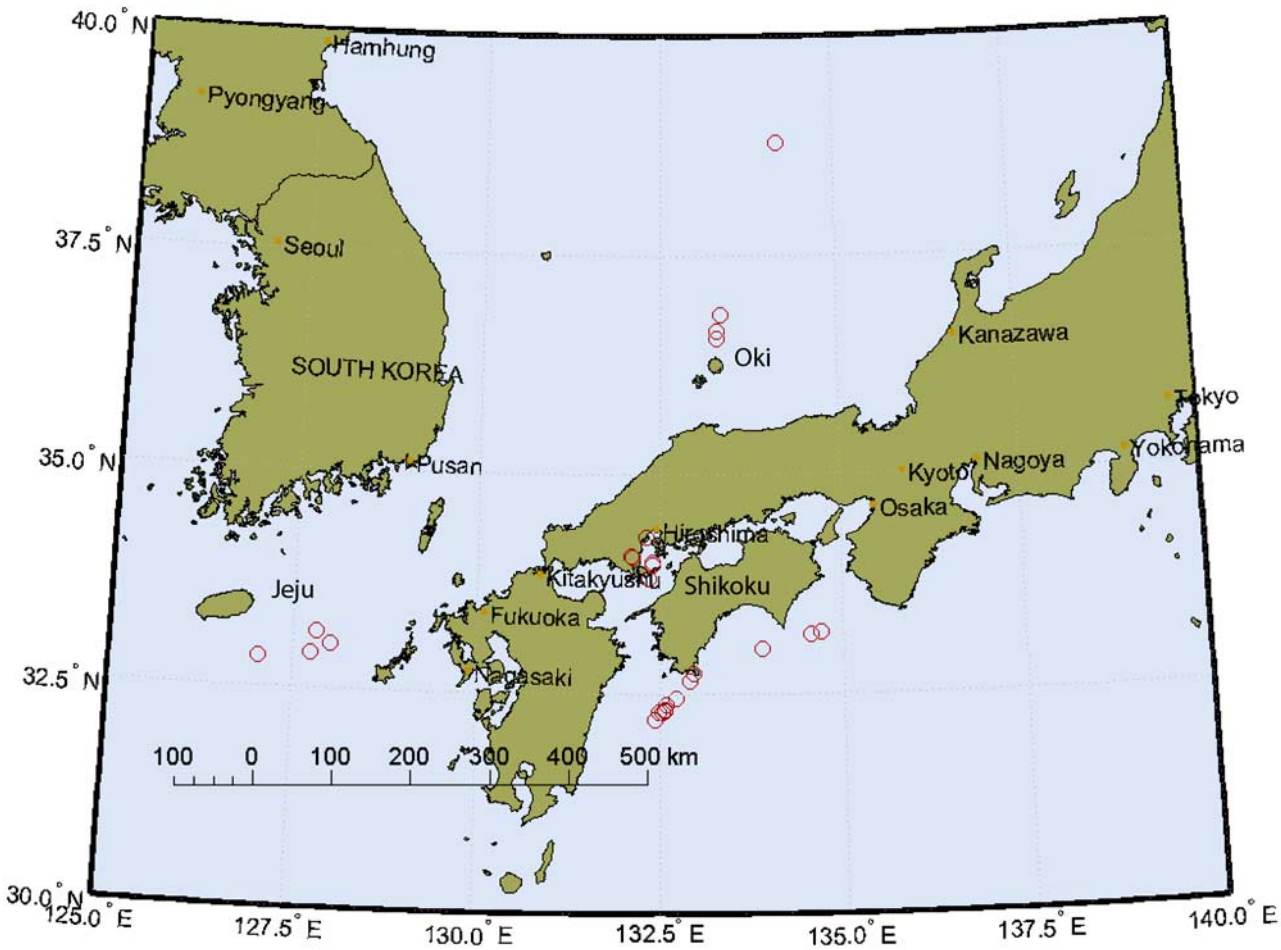

Figure 1. Location of 26 aerosol and water vapor vertical profiles obtained with AATS-14 during ACE-Asia.

[12] The ACE-Asia AATS-14 data set consists of 13 wavelengths (354, 380, 449, 499, 525, 606, 675, 778, 864, 1019, 1059, 1241, and 1558 nm) at which we retrieve $\tau_p(\lambda)$ and the 940-nm wavelength, which we use to determine CWV [*Schmid et al.*, 2001].

[13] AATS-14 was calibrated at the Mauna Loa Observatory (MLO), Hawaii, two months before and one month after the ACE-Asia campaign using the Langley plot technique [*Schmid and Wehrli*, 1995]. As a result of bandpass filter degradation, the calibration constants obtained from the post-mission calibration were lower than those obtained from the pre-mission calibration. However, for eight of the 14 wavelengths the change was only 0.5% or less. Five aerosol channels (354, 380, 449, 525, and 606 nm) had degraded by 0.9 to 3.2%. Note that

$$\Delta\tau_p(\lambda) = \frac{1}{m}\frac{\Delta V_0(\lambda)}{V_0(\lambda)} \tag{1}$$

with

$$m \approx \frac{1}{\cos\theta} \tag{2}$$

Hence a relative uncertainty of 1% in the calibration constant V_0 will lead to an absolute uncertainty in the aerosol optical depth $\Delta\tau_p(\lambda)$ of 0.01 for a solar zenith angle $\theta = 0°$.

[14] To determine the most plausible set of calibration constants applicable to the ACE-Asia data set we inspected $\tau_p(\lambda)$ spectra measured during higher-altitude legs (typically around 3.5 km). We focused on the days with the lowest $\tau_p(\lambda)$ (0.03 to 0.14 at 499 nm, at around 3.5 km altitude). This resulted in 14 spectra taken during 13 flights. It should be noted that although these were the lowest $\tau_p(\lambda)$ we observed at 3.5 km the values are well above a typical background (during the February and June 2001 calibrations at MLO at about the same altitude above sea level we found $0.007 < \tau_p(499\text{ nm}) < 0.023$), revealing the prevalence of dust layers above that altitude. Starting with calibration constants obtained by linearly interpolating $V_0(\lambda)$ between pre- and post-mission calibration, we then adjusted the calibration constants within the bounds of pre- and post-mission calibration in such a fashion that the retrieved $\tau_p(\lambda)$ yielded "smooth" $\tau_p(\lambda)$ spectra for all 14 high-altitude cases. This procedure revealed that for five channels the pre-mission calibration was best, whereas for the remaining channels the interpolated calibration was

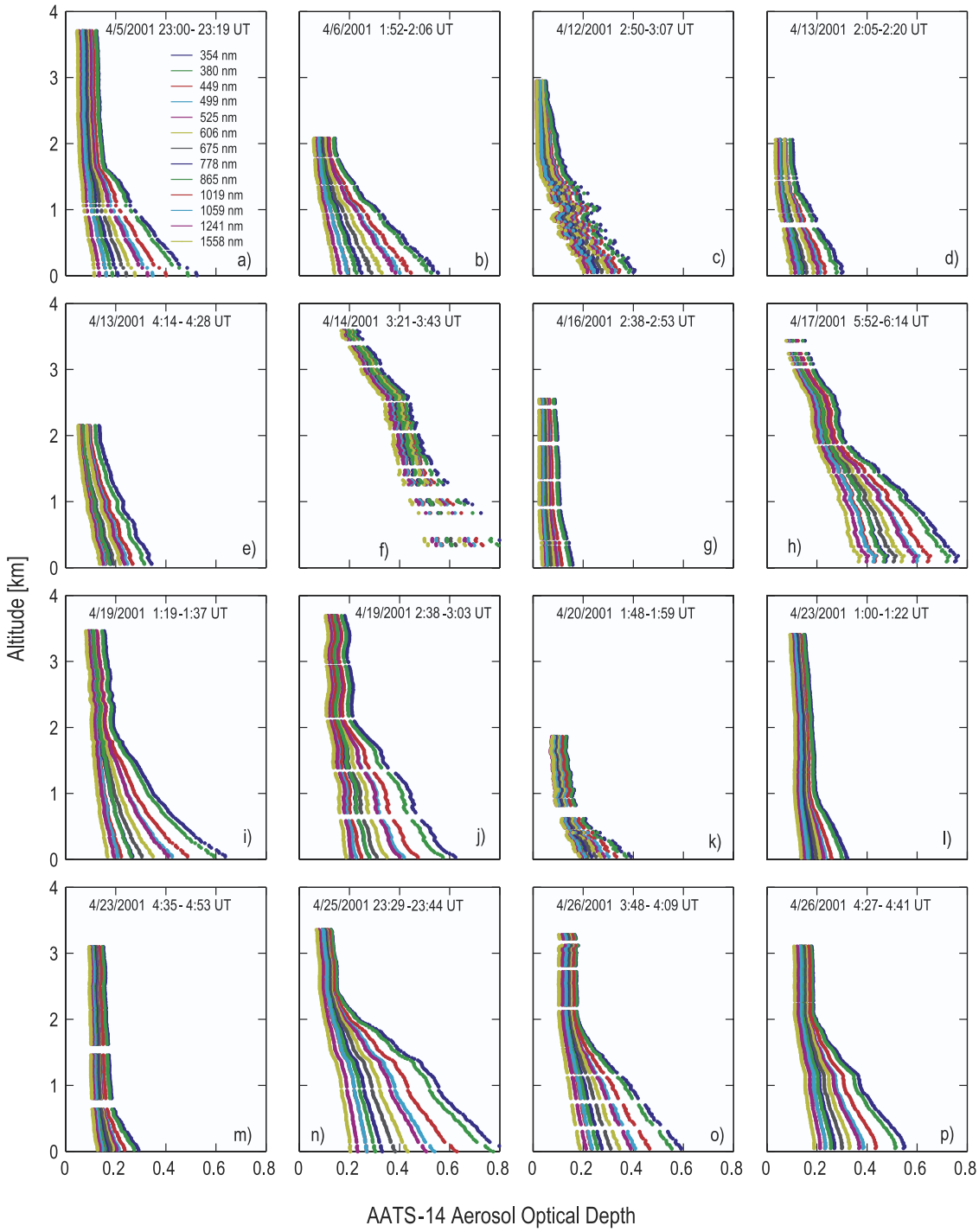

Figure 2. (a–p) Selection of $\tau_p(\lambda)$ vertical profiles from AATS-14 during ACE-Asia.

appropriate. The 606-nm channel (which degraded most, 3.2%) required us to use one value of V_0 for flights 1 through 9 and a lower value for the remaining flights. This fine-tuning of the calibration constants indicates that some of the optical filters must have degraded in a stepwise fashion.

[15] Because of the large transmission loss of the 606-nm bandpass filter (the AATS-14 channel most sensitive to ozone) and hence large calibration uncertainty, the ozone retrieval was turned off for the results shown here and the total column ozone values were taken from the Total Ozone Mapping Spectrometer (TOMS) on the Earth Probe satellite.

[16] The total uncertainty of the retrieved $\tau_p(\lambda)$, due to uncertainties in calibration, sun-tracking, signal measurement, air mass computation, and corrections of molecular scattering and absorption, was computed following the procedures given by *Russell et al.* [1993a]. The uncertainty in CWV was computed following *Schmid et al.* [1996]. During ACE-Asia, AATS-14 sampled at 3 Hz with data recorded every 4 seconds s consisting of an average of

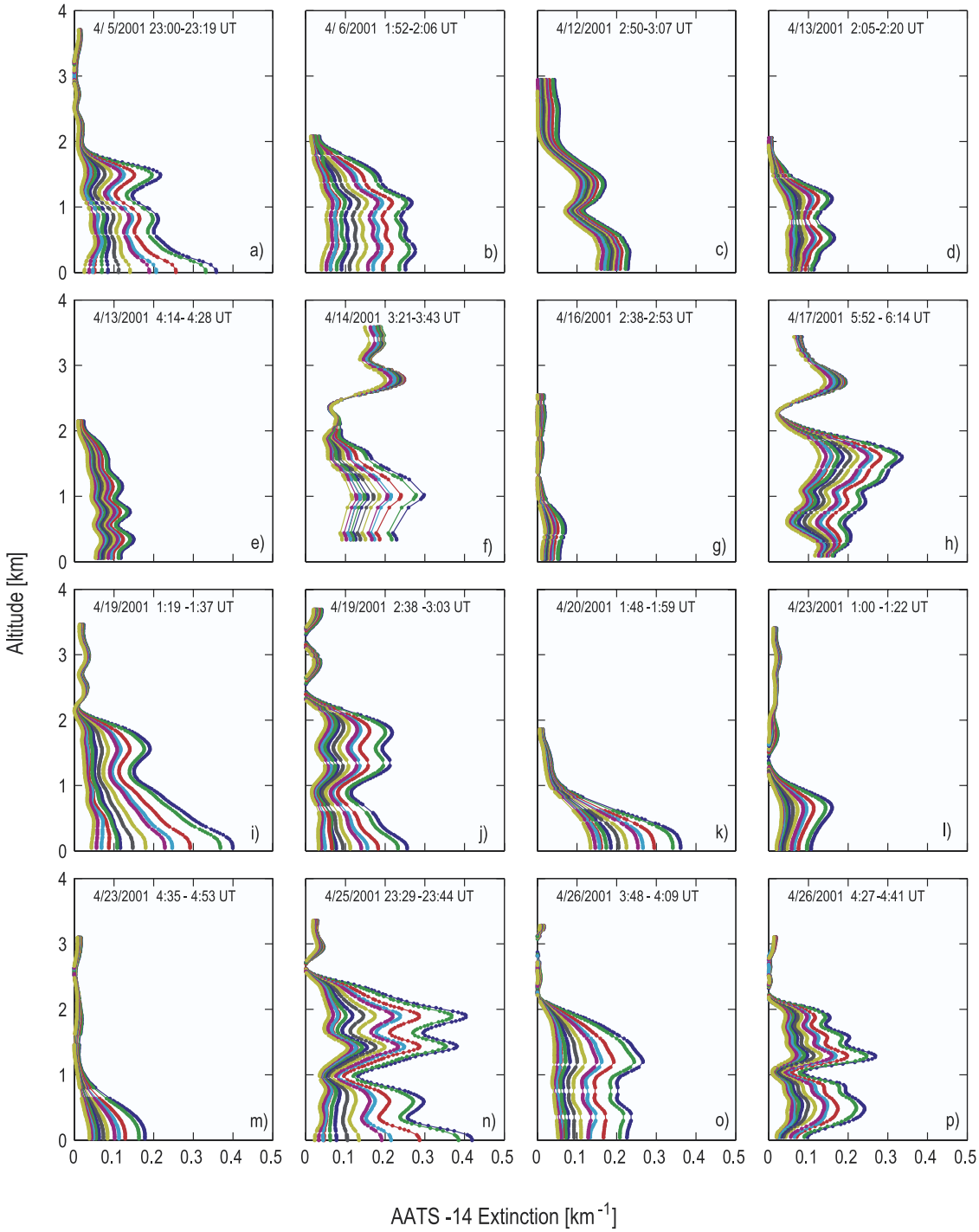

Figure 3. (a–p) Vertical profiles of $\sigma_{ep}(\lambda)$ derived from the $\tau_p(\lambda)$ profiles shown in Figure 2.

9 samples taken in the first 3 of the 4 seconds. The sample standard deviation of all science detector outputs is also stored in the data files. These standard deviations were used in our cloud-screening algorithm that is based on clouds exhibiting higher standard deviations than clear sky. This cloud-screening method can be ambiguous when thick and highly variable dust layers are present above the aircraft. However, such cases are not included here, as AATS-14 profile data taken under such conditions are difficult to interpret (we will return to this point later).

[17] The Twin Otter was able to fly as low as 20 m above the ocean surface, thus allowing measurement of the entire overlying atmospheric column. Flying at different altitudes over a fixed location allows derivation of layer $\tau_p(\lambda)$ or CWV. Differentiation of $\tau_p(\lambda)$ or CWV data obtained in vertical profiles allows derivation of spectral aerosol extinction $\sigma_{ep}(\lambda)$ and water vapor density ρ_w.

[18] Because Sun photometers have a nonzero field of view (FOV), they measure some diffuse light in addition to the direct solar beam. As a result, uncorrected Sun photom-

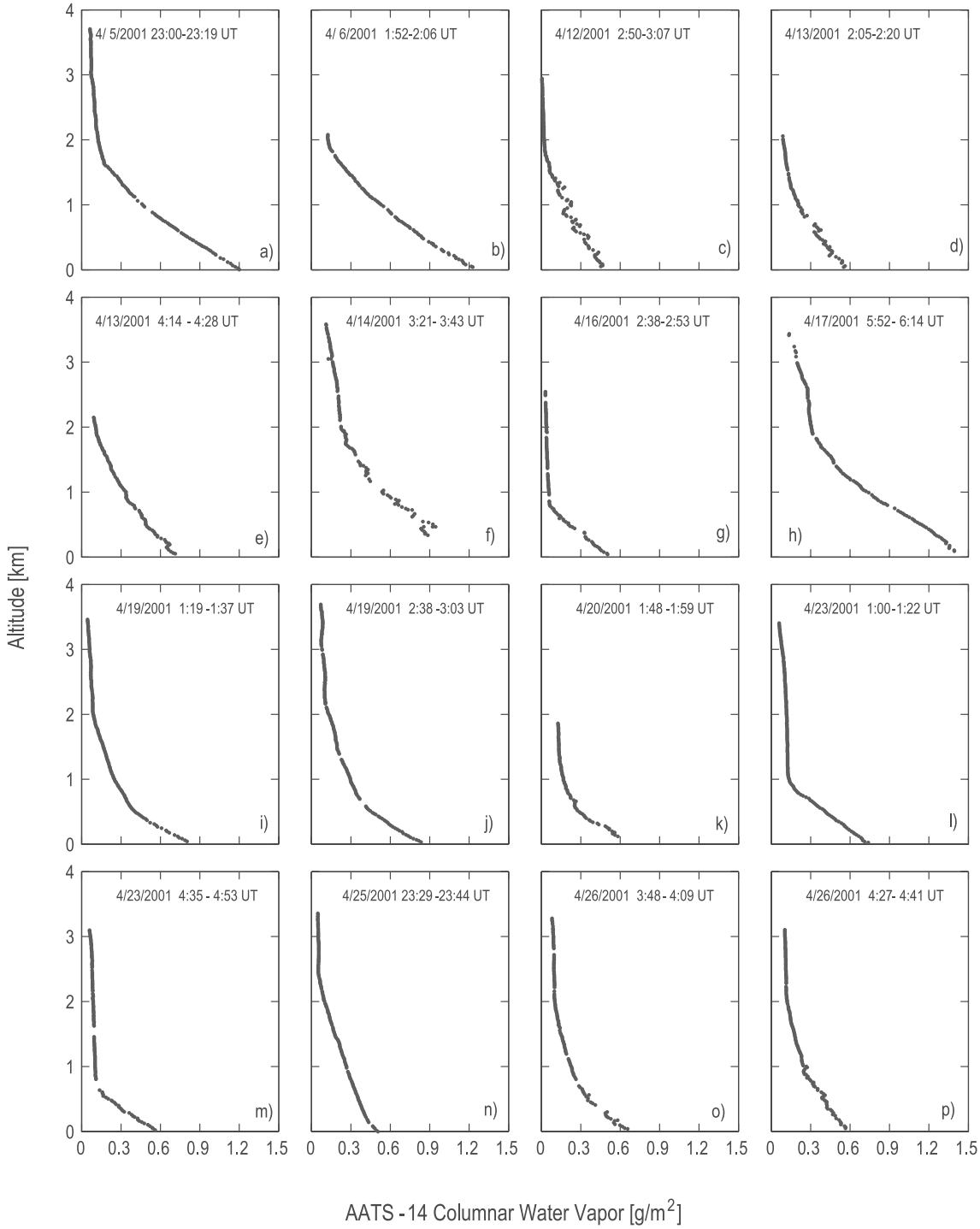

Figure 4. (a–p) Vertical profiles of CWV for cases shown in Figure 2.

eter measurements can overestimate direct-beam transmission and hence underestimate $\tau_p(\lambda)$. For most aerosol conditions and Sun photometer FOVs these effects are negligible. For example, *Eck et al.* [1999] report that for the AERONET sun/sky radiometers, which have FOV half-angle 0.6°, the diffuse-light correction to apparent $\tau_p(\lambda)$ is <0.7% of $\tau_p(\lambda)$, even for desert dust with effective (area-weighted) radius as large as 1.75 μm. The Ames Airborne Tracking Sun photometers, AATS-6 and -14, are designed and built with a relatively large FOV (measured half-angle 1.85°) to help keep the full solar disk in view when sun-tracking during aircraft maneuvers. This larger FOV makes it necessary to assess quantitatively the diffuse light effects on AATS-derived $\tau_p(\lambda)$ when large particles are dominant. We have previously done this for postvolcanic stratospheric aerosols [*Russell et al.*, 1993a, 1993b] and for the Saharan dust encountered in the Puerto Rico Dust Experiment (PRIDE) [*Livingston et al.*, 2003].

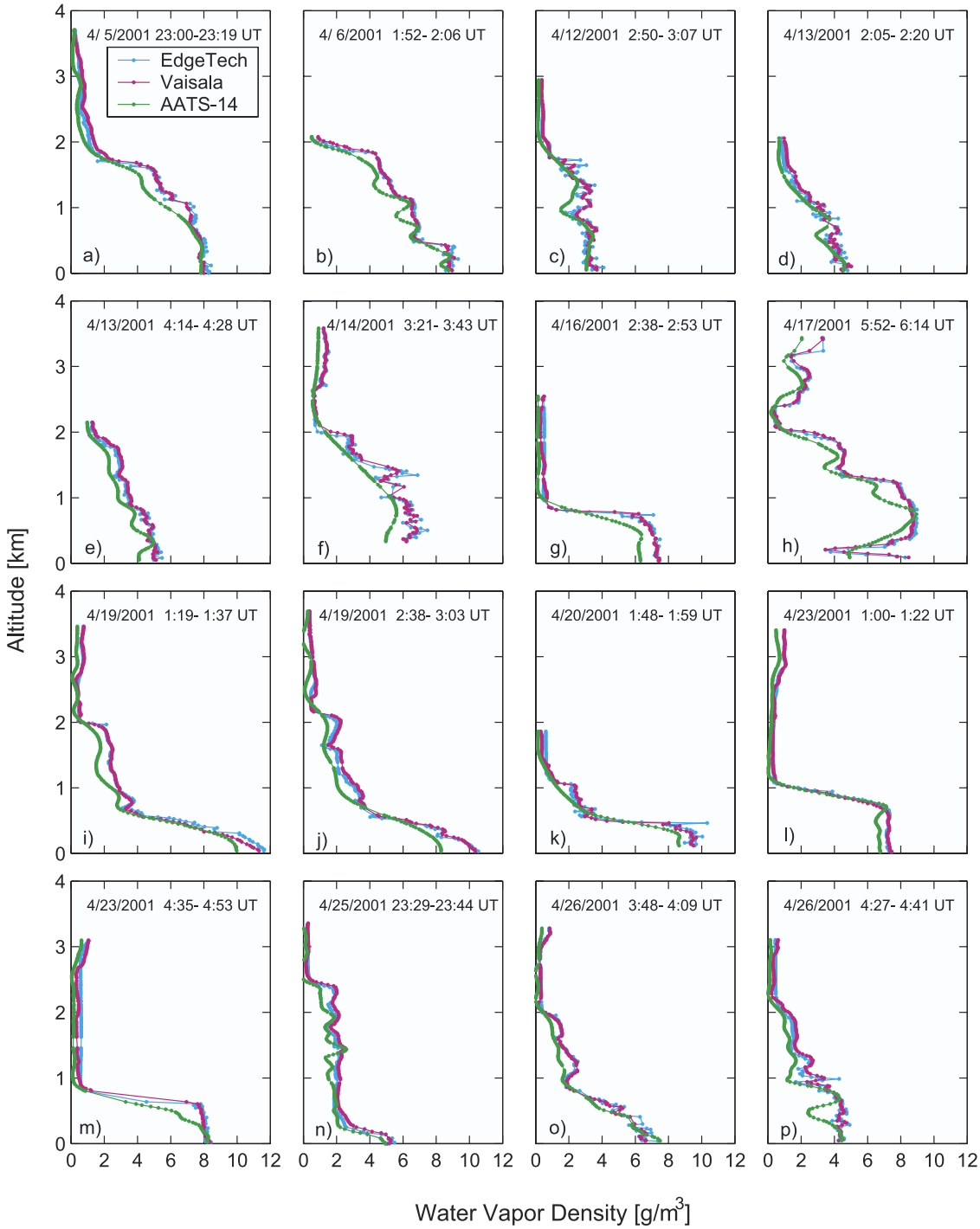

Figure 5. (a–p) Vertical profiles of ρ_w from AATS-14, and EdgeTech and Vaisala in situ sensors for the cases shown in Figure 4.

[19] To quantify the diffuse light effects for the aerosols prevalent during ACE-Asia we used the analytical formulation of *Shiobara and Asano* [1994] and *Kinne et al.* [1997] to calculate $\tau_p(\lambda)$ correction factors

$$C = \tau_p(\lambda)/\tau_p(\lambda)' \tag{3}$$

where $\tau_p(\lambda)'$ is apparent (uncorrected) $\tau_p(\lambda)$. Our calculations used the AATS-14 FOV (half-angle 1.85°) and aerosol scattering phase functions derived both from (1) relative size distributions and complex refractive indices retrieved from Sun and sky radiance measurements by AERONET stations [*Holben et al.*, 1998; *Dubovik et al.*, 2002] in the ACE-Asia region during Spring 2001, and (2) relative size distributions and compositions measured on the Twin Otter in ACE-Asia [*Wang et al.*, 2002]. The correction factors C depend on the fraction of extincted (scattered plus absorbed) light that is scattered into the Sun photometer FOV. This

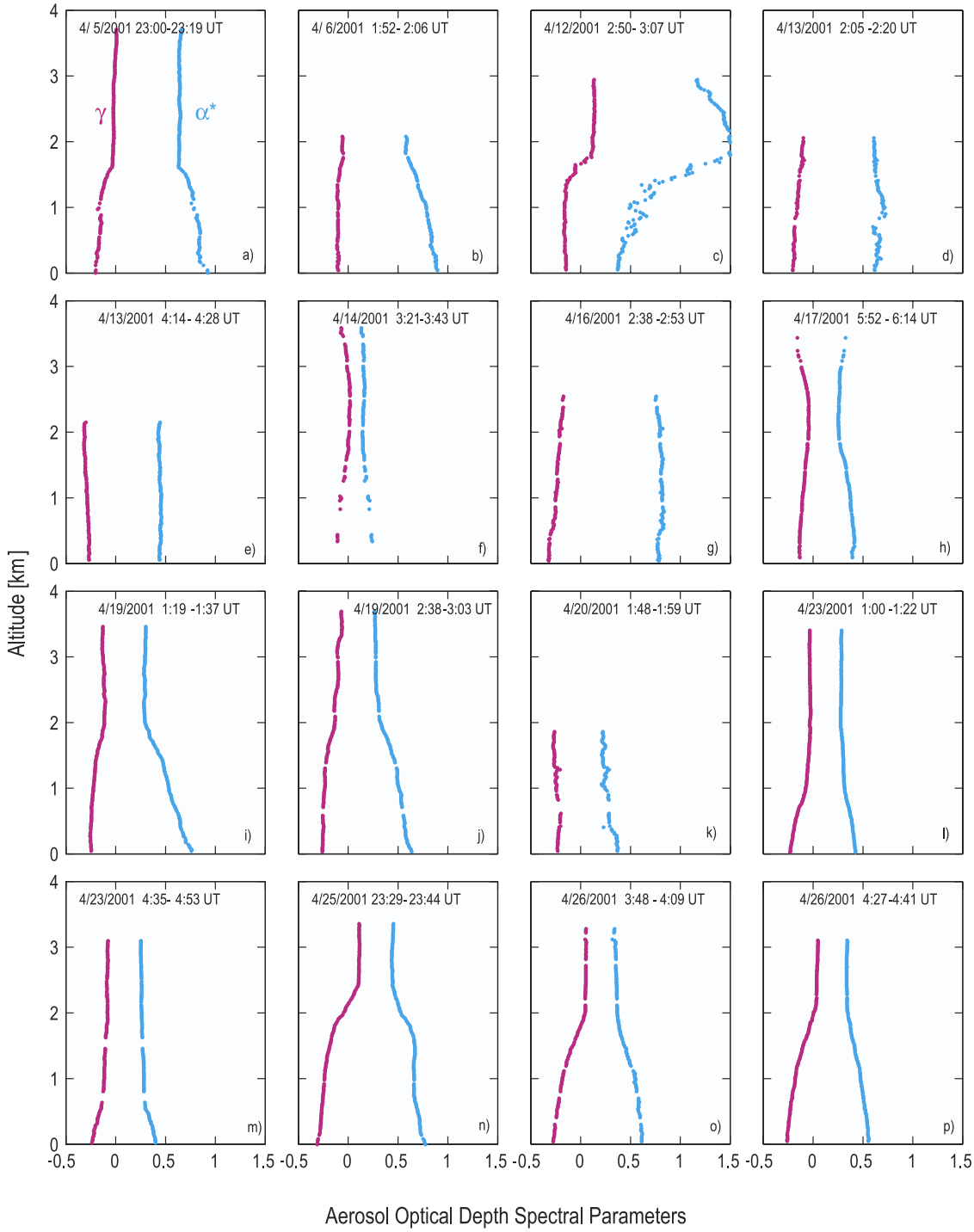

Figure 6. (a–p) Vertical profiles of $\tau_p(\lambda)$ spectral parameters for profiles shown in Figure 2.

fraction (and hence C) increases with decreasing wavelength, because shorter wavelengths have increasingly forward-peaked phase functions. Also, this fraction and C increase as particle size increases (which also increases phase function forward peaking), but they are independent of the absolute number or optical depth of particles on the sun-viewing path [see, e.g., *Shiobara and Asano*, 1994; *Kinne et al.*, 1997; *Box and Deepak*, 1979]. Thus they depend on relative size distributions but not absolute distributions.

[20] We found that the correction factors were well correlated with aerosol effective (area-weighted) radius and also with Ångström exponent

$$\alpha(\lambda_1, \lambda_2) = -\ln\left[\tau_p(\lambda_1)/\tau_p(\lambda_2)\right]/\ln(\lambda_1/\lambda_2). \quad (4)$$

The correlation with α improved as wavelengths λ_1 and λ_2 increased. (Evidently this is because longer wavelengths are

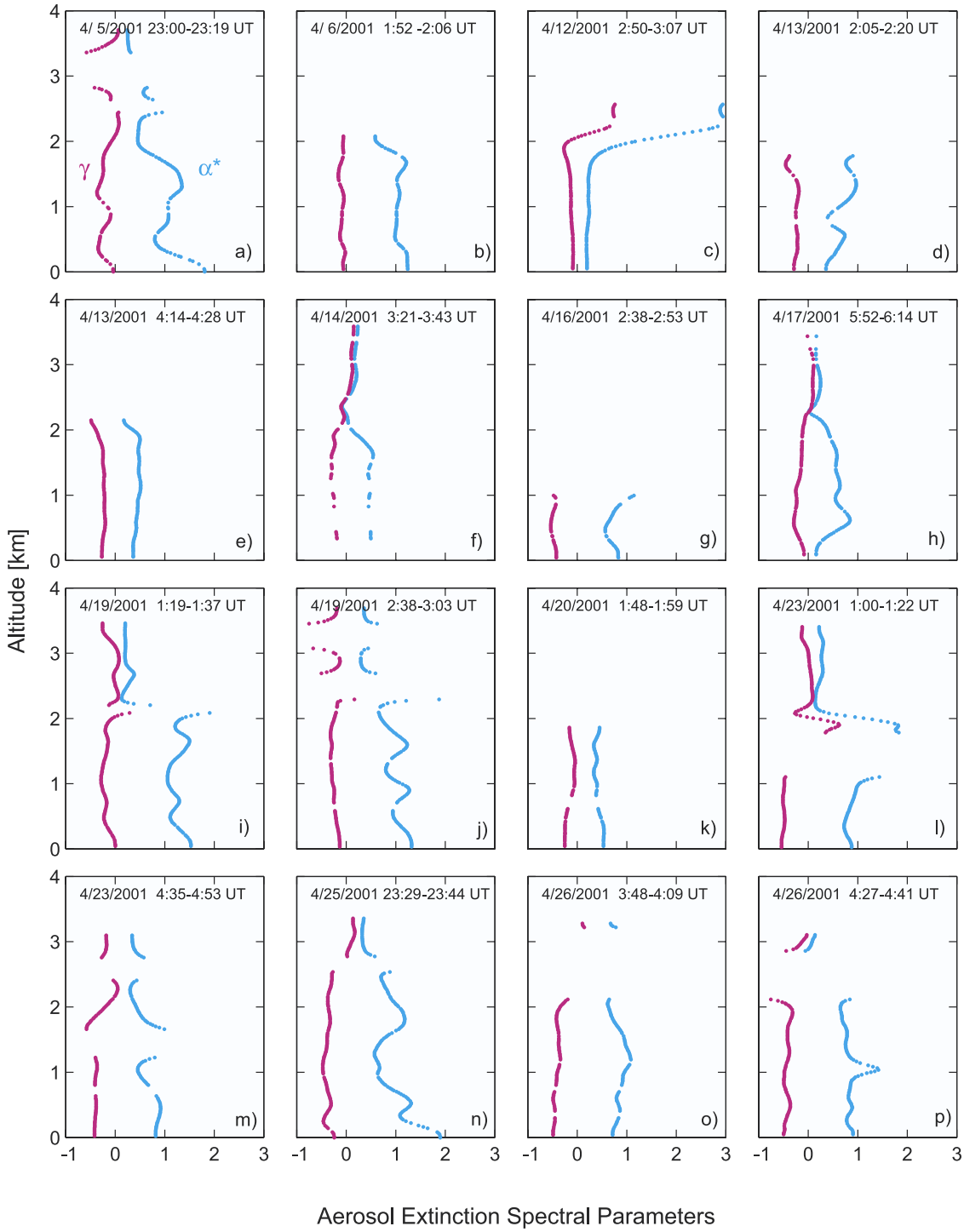

Figure 7. (a–p) Vertical profiles of $\sigma_{ep}(\lambda)$ spectral parameters for profiles shown in Figure 3.

more sensitive to the larger particles in a distribution, and the larger particles are responsible for the diffuse light effects). Scatterplots of C-1 versus α, which included results from both the AERONET and Twin Otter data sets mentioned above, were well fitted by exponentials of the form

$$f = C - 1 = A \exp(-B\alpha). \quad (5)$$

Hence we corrected each individual $\tau_p(\lambda)'$ measurement using these fitted exponential functions and the α value of the overlying aerosol column (using λ_1 = 1020 nm and λ_2 = 1558 nm). As noted above, the correction factor f decreases with increasing wavelength. For the shortest AATS-14 wavelength (354 nm), 90% of all τ_p' had to be corrected by less than 6%, with 60% of all τ_p' requiring less than 4% correction. To illustrate, a 4% correction to τ_p' = 0.3 is 0.012. Uncertainties in the diffuse-light correction factors,

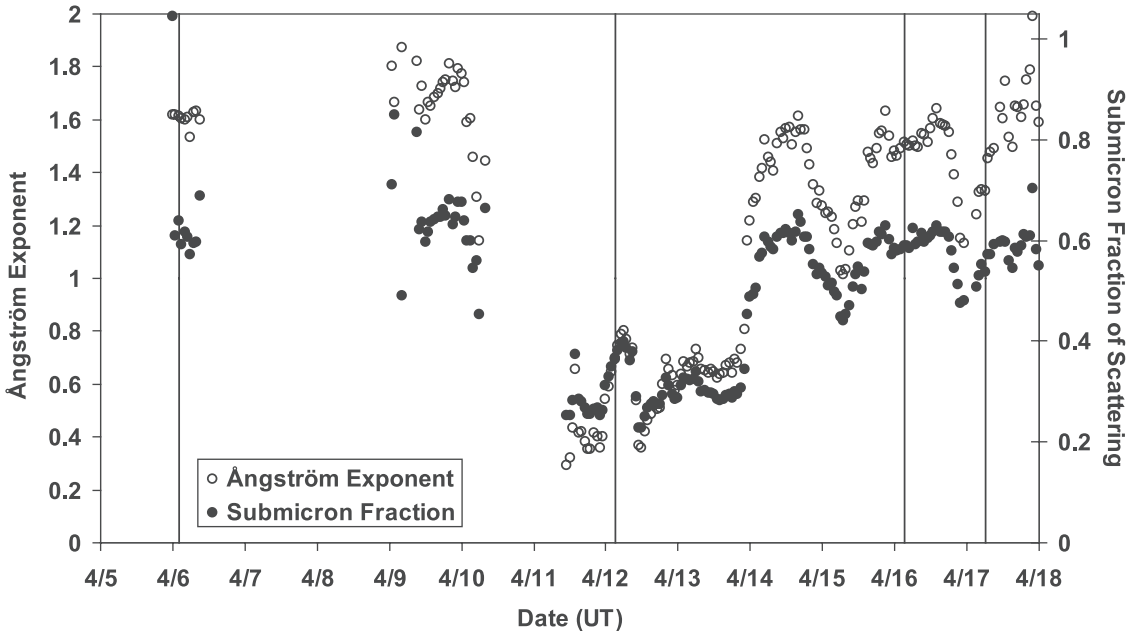

Figure 8. Sub-μm fraction of scattering, FF_{sp} (550 nm), and Ångström exponent α_{sp} (450, 700 nm) from sub-10-μm scattering, obtained from ground-based TSI model 3563 nephelometer measurements at Gosan on Jeju island (South Korea). Missing data on 10 and 11 April are due to a power outage in the measurement trailer. Vertical lines indicate times of Twin Otter vertical profiles flown just east of Jeju Island.

based on the standard deviations of α-grouped values of C calculated from the AERONET and Twin-Otter data sets, were included in the overall uncertainty of $\tau_p(\lambda)$ using equation (A22a) of *Russell et al.* [1993b].

2.1.3. Aerosol Extinction From Airborne Scattering and Absorption Measurements

[21] Light-scattering data were obtained from four integrating nephelometers aboard the Twin Otter. One of these was a TSI model 3563 three wavelength (450, 550, 700 nm), integrating nephelometer and the other three were Radiance Research (RR) model 903 single wavelength (550 nm) nephelometers. All four nephelometers were calibrated against particle-free air and CO_2 prior to the field deployment and zeroed with particle-free air before each flight. All of the nephelometers sampled from a shrouded intake whose nominal 50% cutoff diameter was determined to be 8 μm (determined by comparison of cross-calibrated interior and exterior FSSP-100 optical probes [*Gao et al.*, 2003]). The three model 903 nephelometers were operated at relative humilities (RH) near ambient, ca. 30% below ambient and near 85%. The TSI nephelometer was operated ca. 30% below ambient as well.

[22] The RR nephelometer operating closest to ambient RH was selected as the light-scattering signal. All nephelometers were corrected for truncation and illumination as suggested by *Anderson and Ogren* [1998] utilizing the Ångström coefficient from the TSI nephelometer but with an angular truncation for the RR nephelometers based on actual measurements of the scattering geometry of the RR nephelometers since this geometry differs significantly from that of the TSI instrument.

[23] The hygroscopic behavior of the aerosol was determined from the three RR nephelometers operating at different RH. The dependence of light-scattering on RH, $f(\sigma_{sp}(RH))$, was parameterized by the exponent of equation (6), based on the work of *Kasten* [1969; see also *Gassó et al.*, 2000].

$$\sigma_{sp}(RH) = \sigma_{sp}(RH_0)\left(\frac{100 - RH}{100 - RH_0}\right)^{-\gamma} \tag{6}$$

where the zero subscript refers to some low, reference RH, and the exponent, γ, for the measured dependence of light-scattering on RH, is determined by fitting the data to equation (6) as given by *Gassó et al.* [2000]. We then utilized γ to correct the near-ambient RR nephelometer scattering signal to the measured ambient RH.

[24] Aerosol light absorption was also measured using an absorption photometer (model PSAP) made by Radiance Research (Seattle, WA) utilizing the data reduction scheme of *Bond et al.* [1999]. Because the absorption was measured just downstream of the TSI nephelometer, it was measured under sub-ambient RH (a nominal 30% below ambient). However, following *Hegg et al.* [1997], no correction was made for the higher RH of the ambient air since experimental data for such a correction are lacking. A study modeling sulfates with black carbon cores by *Redemann et al.* [2001] suggests that absorption humidification factors are negligible for a wide range of atmospheric conditions. However, this may not apply to the considerably more complex Asian aerosol.

[25] Both the scattering and absorption signals were filtered to eliminate data points below the detection limit of the instruments (e.g., 0.003 km^{-1} for the TSI nephelometer) and clearly erroneous values generated by intermittent dropouts of components of the instruments on which the

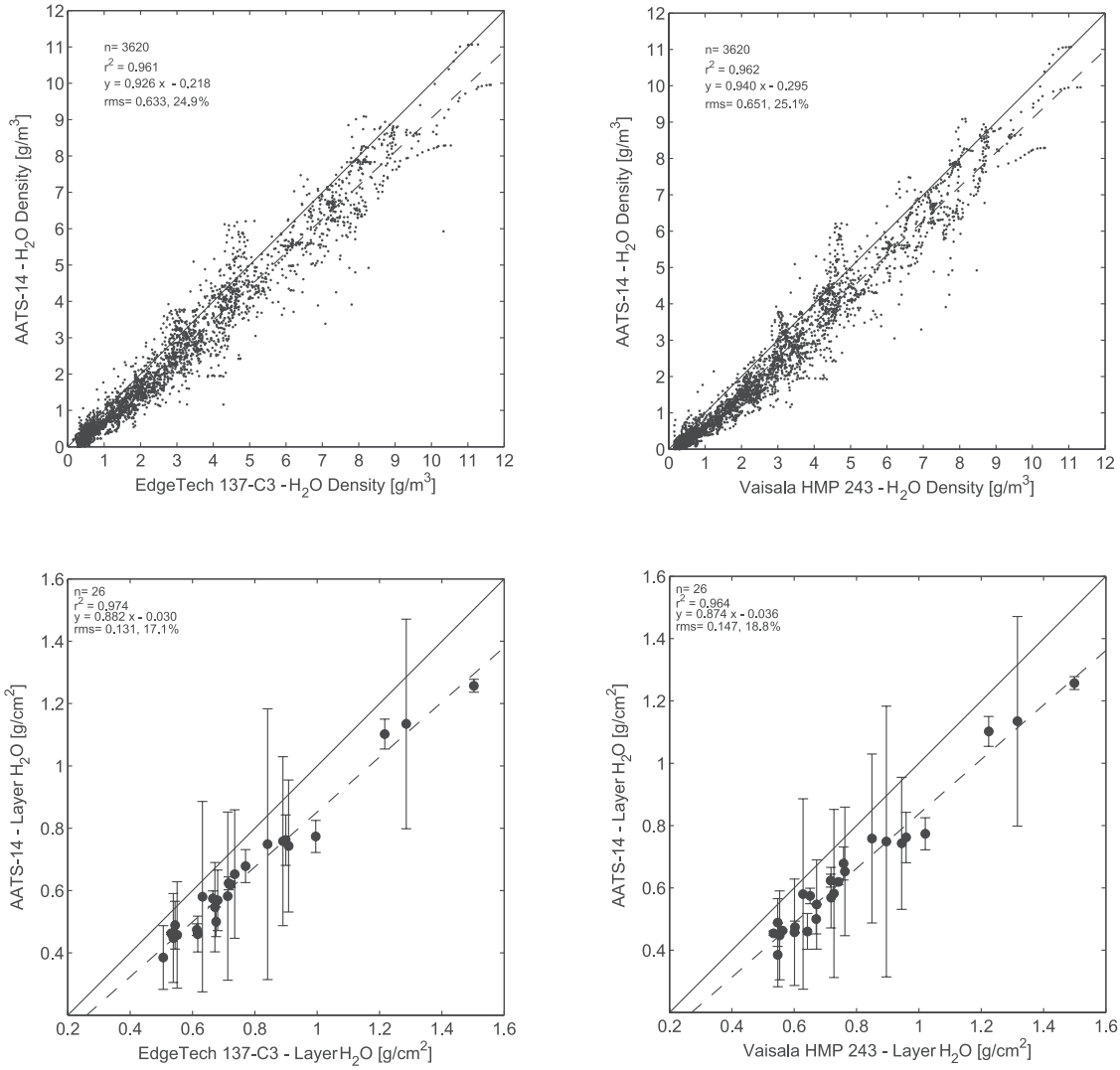

Figure 9. Comparison of water vapor density (upper row) and layer water vapor (lower row) from AATS-14, EdgeTech 137-C3 Chilled Mirror and Vaisala HMP 243 humidity sensor for 26 vertical profiles. Error bars are based on horizontal distance spanned by a profile, combined with average horizontal variability of CWV in ACE-Asia flights.

overall signal is dependent (e.g., the RH sensors in the nephelometers). Furthermore, it was necessary to eliminate some of the PSAP data because of the sensitivity of the instrument to rapidly changing ambient pressure and instrument humidity, encountered during some of the spiral ascents and descents used to generate the vertical profiles of in situ parameters. After such filtering, the absorption and scattering signals were added together to produce the extinction coefficient at 550 nm.

[26] The number of data points eliminated by the above filtering procedure was, in some cases, fairly high (~20%) and in all cases resulted in an irregular spacing of data points with respect to altitude. This presents a problem for vertical integration of the extinction coefficient to obtain the layer $\tau_p(\lambda)$ since normal Gaussian quadrature requires an even spacing of data points. Hence the measured values of extinction were interpolated to a regularly spaced grid using a cubic interpolation algorithm. The in situ profiles shown in the analysis and compared to the Sun photometer measurements are these interpolated profiles.

2.1.4. Aerosol Extinction From Airborne Size Distribution and Composition Measurements

[27] Aerosol size distributions and chemical compositions were measured using differential mobility analyzers, an aerodynamic particle sizer, Micro-Orifice Uniform Deposit Impactors, and denuder samplers onboard the Twin Otter aircraft as part of the ACE-Asia campaign [*Wang et al.*, 2002]. Of the 19 research flights, measurements on 4 flights that represented four specific and different aerosol characteristics were analyzed in detail by *Wang et al.* [2002]. They compared $\sigma_{ep}(\lambda)$ predicted using in situ aerosol size distribution and chemical composition measurements to those derived from AATS-14. For this paper we have rerun these computations for λ = 550 nm to put them in the additional context of σ_{ep}(550 nm) derived from

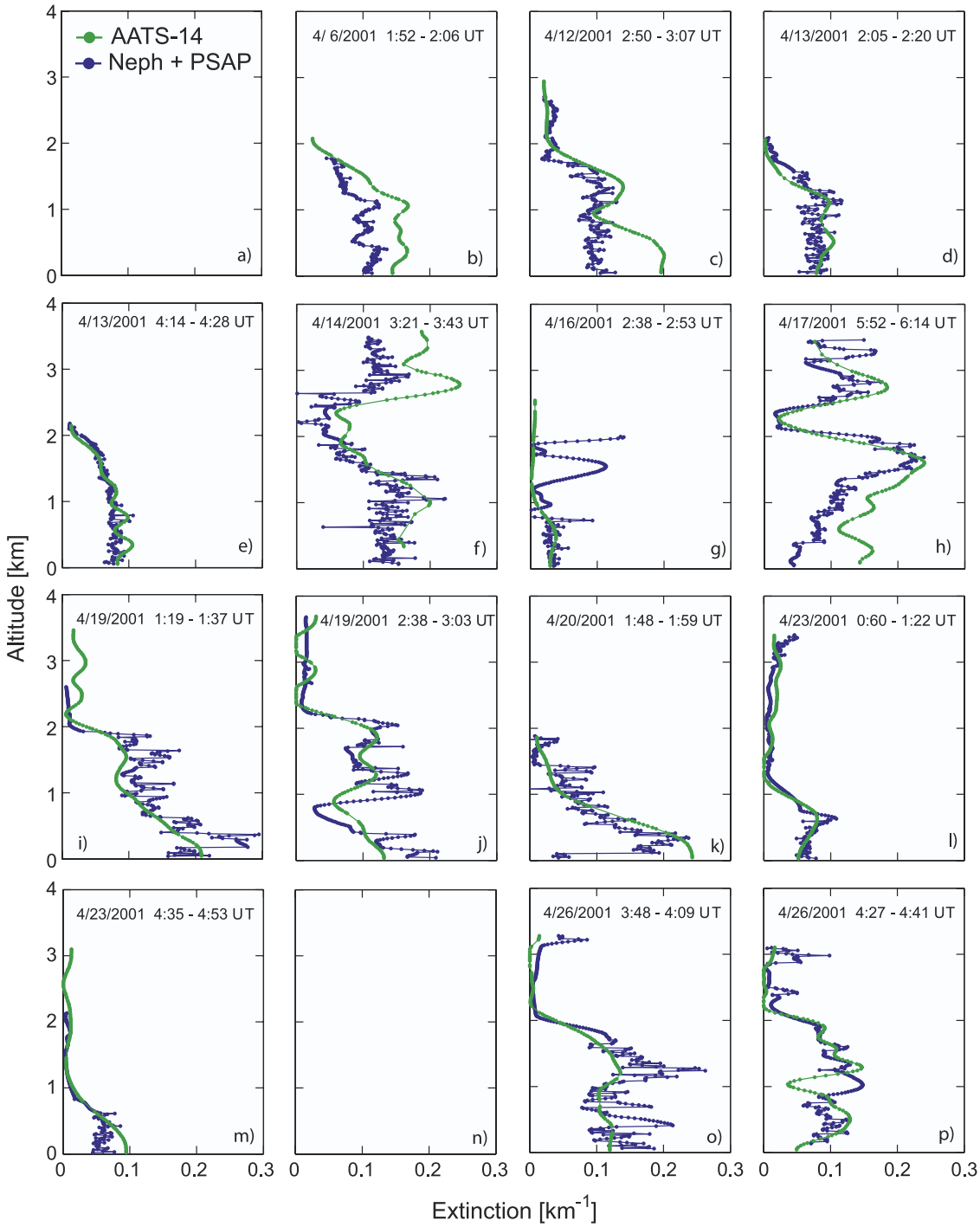

Figure 10. (a–p) Vertical profiles of σ_{ep}(550 nm) from AATS-14 and the sum of scattering and absorption from Nephelometers and PSAP instruments.

airborne scattering and absorption measurements, and from ship based lidar measurements.

2.2. Aerosol Extinction From Shipborne Lidar Measurements

[28] The Micro-Pulse Lidar (MPL) [*Spinhirne et al.*, 1995] is a single channel (523 nm), autonomous, eye-safe lidar system originally developed at the NASA Goddard Space Flight Center and is now commercially available. MPLNET [*Welton et al.*, 2001] is a worldwide network of ground-based MPL systems, co-located with AERONET Sun/sky radiometers [*Holben et al.*, 1998]. The MPL is used to determine the vertical structure of clouds and aerosols. The MPL data are analyzed to produce optical properties, such as extinction and optical depth profiles of clouds and aerosols. During ACE-Asia, an MPL system was operated aboard a ship, the R/V *Ronald H. Brown*.

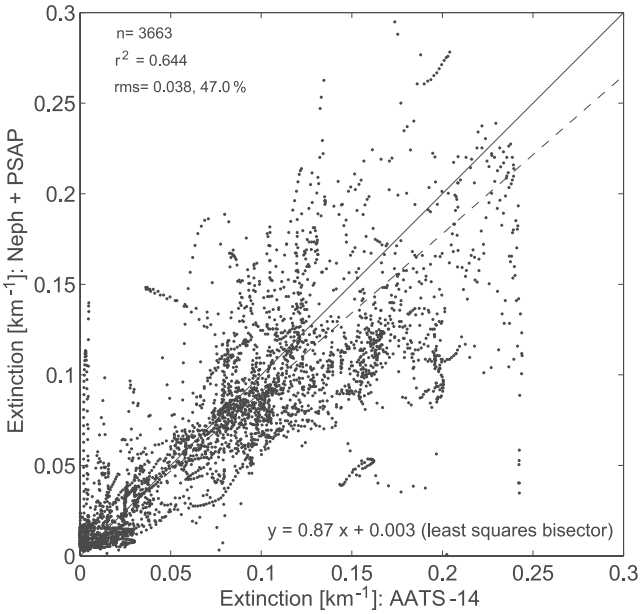

Figure 11. Comparison of σ_{ep}(550 nm) from AATS-14 and the sum of scattering and absorption from Nephelometers and PSAP instruments for 14 profiles shown in Figure 10.

[29] The inversion of data from any conventional elastic backscatter lidar (such as an MPL) faces an inherently ill-posed problem, in that it requires the extraction of two unknowns (extinction and 180°-backscatter coefficients) from one measurement (the attenuated 180°-backscatter signal) [*Ackermann*, 1998; *Murayama et al.*, 2003]. In the standard MPLNET processing, the lidar-derived σ_{ep}(523 nm) profile is obtained by the *Fernald* [1984] backward two-component algorithm assuming an altitude-independent lidar ratio, S_p, (σ_{ep} divided by 180°-backscatter) and constrained by the total column τ_p(523 nm) measured with the AERONET Sun/sky radiometer at the MPLNET site. For MPLNET measurements carried out on ships, τ_p(523 nm) is obtained from shipborne Sun photometers.

3. Results

3.1. AATS-14 Vertical Profiles

[30] During ACE-Asia, AATS-14 measured numerous vertical profiles of $\tau_p(\lambda)$ and CWV. After discarding profiles influenced by considerable spatial inhomogeneity or overlying clouds we derived spectral aerosol extinction $\sigma_{ep}(\lambda)$ and water vapor density ρ_w for 26 profiles by differentiating the $\tau_p(\lambda)$ and CWV profiles. The locations of the 26 profiles are shown on the map in Figure 1. Geographically they can be grouped in four areas: ascents or descents out of or into Iwakuni airport, and profiles south of Shikoku Island, just east of Jeju Island, and north of Oki Island. Figure 2 shows a selection of 16 $\tau_p(\lambda)$ vertical profiles. Figure 3 shows the corresponding $\sigma_{ep}(\lambda)$ profiles. The profiles of CWV for the same 16 cases and the corresponding ρ_w profiles are depicted in Figures 4 and 5. To facilitate comparisons we plotted all profiles on the same scale. Gaps in the $\tau_p(\lambda)$ or CWV vertical profiles are caused by temporary blockage of the direct solar beam by aircraft structures (tail, antennas) or overlying clouds. In the case of thin overlying clouds determination of CWV may still be possible (see Figures 2k and 4k).

[31] Most vertical profiles were acquired within 20 min of flight time. Occasionally, $\tau_p(\lambda)$ or CWV decreased (increased) when the plane descended (ascended). In a horizontally homogeneous, time-invariant atmosphere, this would be impossible. However, in the real atmosphere it can occur because (1) the Sun photometer can only measure the transmittance of the Sun photometer-to-sun path, (2) that path in general passes through a horizontally inhomogeneous, time-varying atmosphere, and (3) the path and the atmosphere move with respect to each other as the aircraft moves and the wind blows. Before the Sun photometer $\tau_p(\lambda)$ or the CWV profile is vertically differentiated to obtain $\sigma_{ep}(\lambda)$ or ρ_w, it has to be smoothed (in a non-biased manner) to eliminate increases in $\tau_p(\lambda)$ or CWV with height. In this study we first averaged the $\tau_p(\lambda)$ or CWV values over 20-m altitude bins and then used smoothed spline fits for this purpose. However, to avoid over-smoothing at altitudes that exhibit actual variations of $\tau_p(\lambda)$ or CWV we occasionally allow $\sigma_{ep}(\lambda)$ or ρ_w to become slightly negative, as can be seen in Figures 3 and 5.

[32] The $\tau_p(\lambda)$ profiles in Figure 2 show that the bulk of the optically active aerosols reside below 2 km. However, in many cases the aerosol loading above the ceiling of the Twin Otter is significant (e.g., τ_p(499 nm) ~0.2 in Figure 2f). The $\sigma_{ep}(\lambda)$ profiles in Figure 3 show a considerable amount of layering. When combined with the ρ_w profiles in Figure 5 the vertical extent of the marine boundary layer (MBL) can be identified to be 1–2 km. While in many instances the layering of $\sigma_{ep}(\lambda)$ and ρ_w is similar, significant exceptions do occur (e.g., frames j and n of Figures 3 and 5).

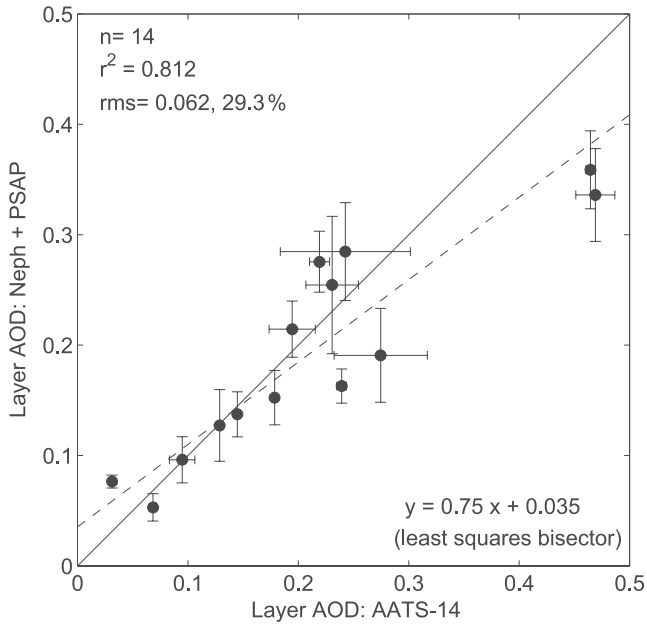

Figure 12. Comparison of layer (top to bottom of profile) τ_p(550 nm) from AATS-14 and the sum of scattering and absorption from Nephelometers and PSAP instruments for 14 profiles shown in Figure 10.

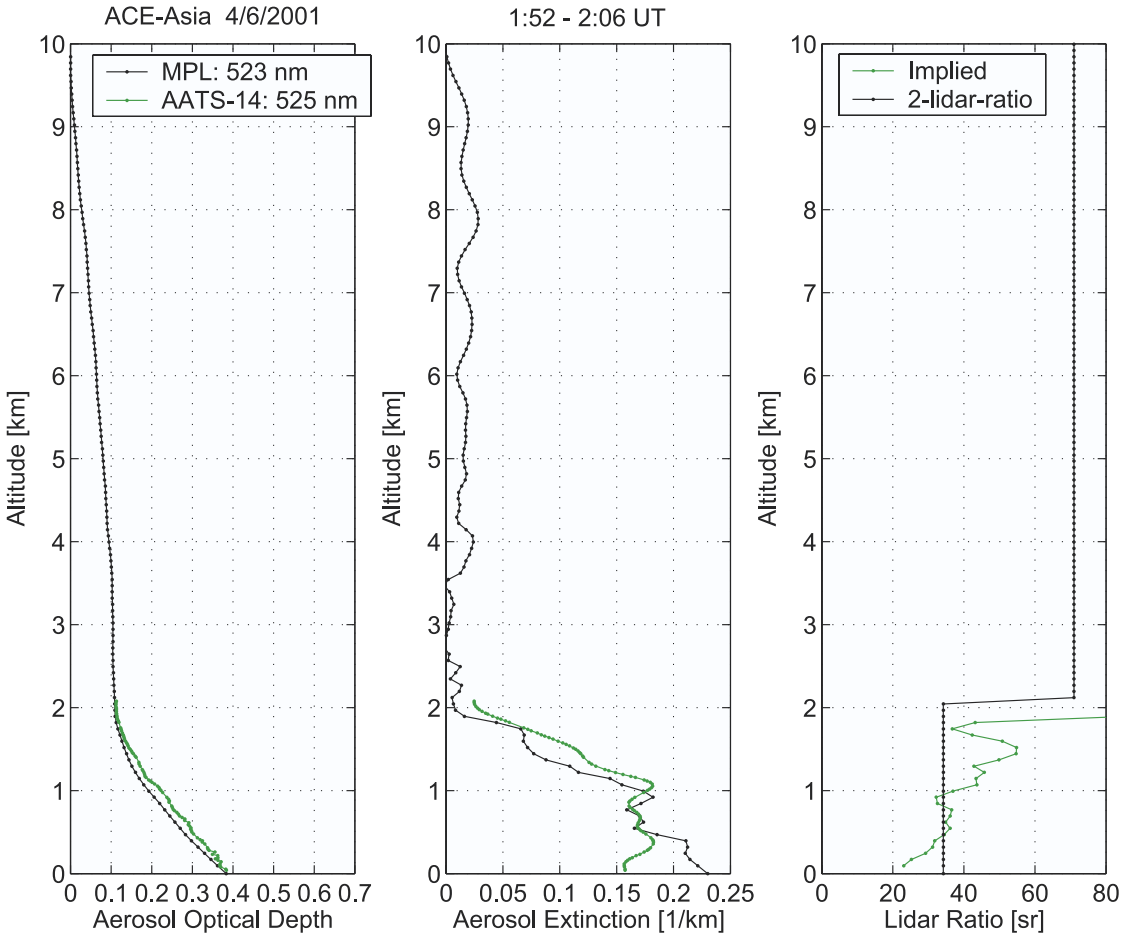

Figure 13. $\tau_p(\lambda)$, $\sigma_{ep}(\lambda)$ and lidar ratio obtained from AATS-14 and ship-based MPL during Twin Otter vertical profile over R/V *Ronald H. Brown* on 6 April 2001.

[33] The water vapor results in Figures 4 and 5 reveal a relatively dry atmosphere during ACE-Asia Twin Otter flights, with all CWV <1.5 cm and ρ_w < 12 g/m^3. The C-130 aircraft encountered similarly dry conditions with the exception of a flight on 30 April 2001 [*Redemann et al.*, 2003]. The Twin Otter did not fly on that day.

[34] Several studies have found that

$$\ln \tau_p(\lambda) = a_0 + a_1 \ln \lambda + a_2(\ln \lambda)^2 \tag{7}$$

yields a very good fit to $\tau_p(\lambda)$ or $\sigma_{ep}(\lambda)$ spectra [*King and Byrne*, 1976; *Michalsky et al.*, 1995; *Eck et al.*, 1999; *Schmid et al.*, 2003]. The spectral parameters α^* and γ shown in Figures 6 and 7were obtained by fitting equation (7) to each AATS-14 $\tau_p(\lambda)$ or $\sigma_{ep}(\lambda)$ spectrum, where $\alpha^* = -a_1$ and $\gamma = -a_2$. In fact, equation (7) is an extension of the traditional Ångström law

$$\tau_p(\lambda) = \beta\lambda^{-\alpha} \tag{8}$$

where the wavelength exponent α is related to the aerosol size distribution [see, e.g., *Schmid et al.*, 1997]. Typically $\sim 0 < \alpha \leq 1$ is found for larger particles and $1 < \alpha \leq \sim 2$ for smaller particles. However, we often find equation (8) to be a poor representation of $\tau_a(\lambda)$, as did the studies mentioned above. Hence we prefer to use equation (7), where α^* is still related to aerosol size and γ describes the curvature of the spectrum (in log-log space) or deviations from equation (8). Of course, if $\gamma = 0$, then equation (7) reduces to equation (8) and $\alpha^* = \alpha$.

[35] In the vertical profiles of α^* and γ derived from $\tau_p(\lambda)$ (Figure 6) we generally observe a decrease of α^* with altitude. This suggests that with increasing altitude $\tau_p(\lambda)$ of the overlying column is increasingly dominated by larger (dust) particles. Typically, the $\tau_p(\lambda)$ spectra are curved concavely ($\gamma < 0$) at lower altitudes and not curved or convexly curved ($\gamma = 0$ or $\gamma > 0$) at higher altitudes.

[36] The vertical profiles of α^*_{ep} and γ_{ep} derived from $\sigma_{ep}(\lambda)$ (Figure 7) show considerably more variation in absolute magnitude (notice change of scale from Figure 6). It can be observed that in the MBL $\gamma_{ep} < 0$ and $\sim 0.5 < \alpha^*_{ep} < 2$, whereas in the free troposphere (FT) often $\gamma_{ep} \cong \alpha^*_{ep} \cong 0$. In fact we find $\gamma_{ep} \cong \alpha^*_{ep} \cong 0$ to be a good indicator for layers dominated by dust particles (most obvious in Figures 7f and 7h). This is corroborated by comparison to in situ size distribution and composition data measured on the Twin Otter [*Wang et al.*, 2002], light scattering data measured aboard the C-130 [*Anderson et al.*, 2003] and on the ground (see below), and also by polarized lidar measurements at several ACE-Asia sites [*Shimizu et al.*, 2003]. As an example, AATS-14 recognizes the layer above 2.2 km on 17 April (Figure 7h) as dust aerosol. The C-130 aircraft

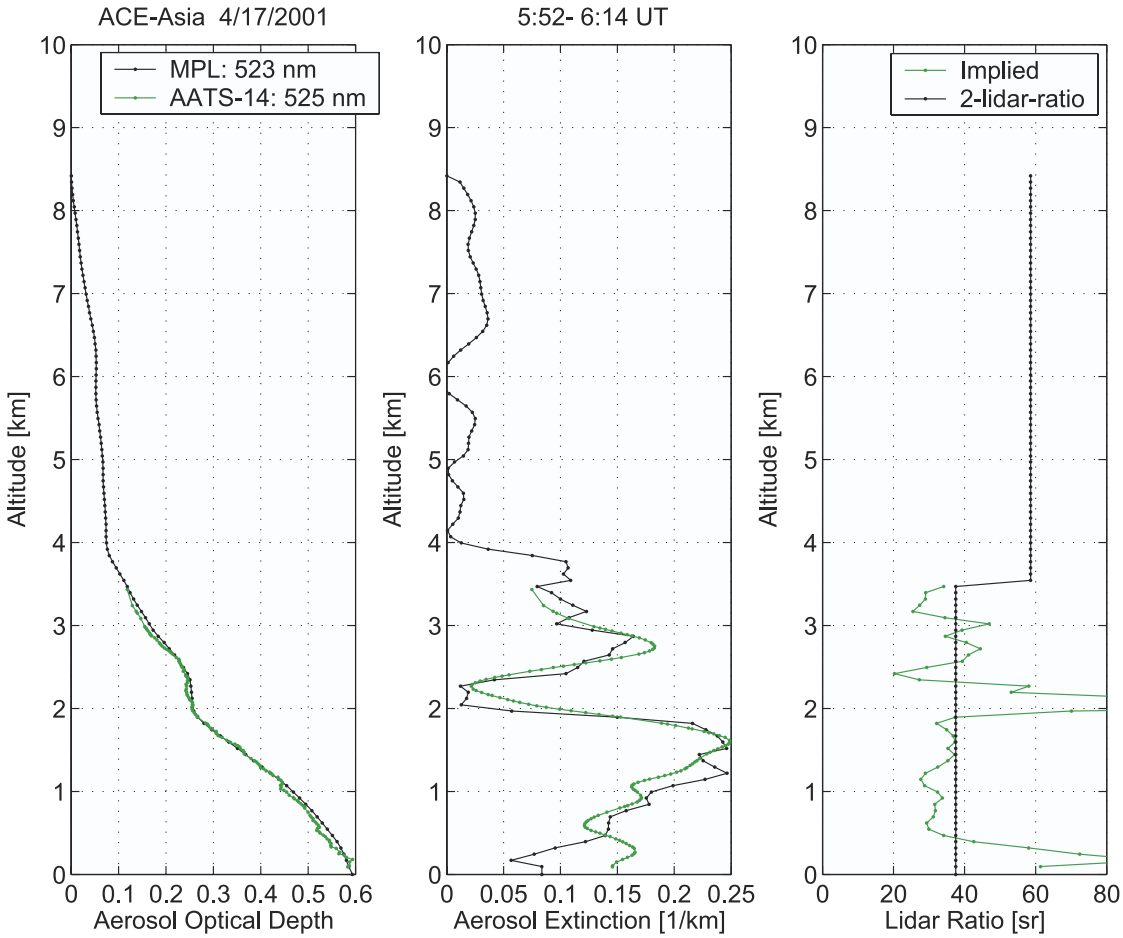

Figure 14. Same as Figure 13 but for 17 April 2001.

flew an ascent from near the surface to 5 km at the same location (i.e., location of the R/V *Ronald H. Brown*) two hours after the Twin Otter profile. The C-130 nephelometer data [*Anderson et al.*, 2003; S. Masonis, personal communication, 2002] show sub-μm fraction of scattering values

$$FF_{sp} = \frac{\sigma_{sp}(D_{aero} \leq 1\ \mu\text{m})}{\sigma_{sp}(D_{aero} \leq 10\ \mu\text{m})} \tag{9}$$

as low as ~0.1 between ~2.5 and 3.25 km clearly identifying that layer as dust.

[37] In the profiles obtained from AATS-14 the layers dominated by dust are usually found in the FT. An exception is the profile in Figure 7c (12 April, flown east of Jeju island), where the AATS-14 data suggest that the aerosol above 1.8 km must be dominated by small pollution or biomass burning particles whereas the dust was mixed into the MBL all the way to the surface. This is confirmed by the sub-μm fraction of scattering, FF_{sp}, and Ångström exponent α_{sp} obtained from ground-based nephelometer measurements at Gosan on Jeju Island. As shown in Figure 8, the measurements on 12 April led to much lower values for both FF_{sp}, and α_{sp} than during any of the other three Twin Otter vertical profiles (Figures 7b, 7g, and 7h) flown in the vicinity of Gosan. The data in Figure 8 and other data from Gosan indicate that the dust reached the surface around 3 UT on 10 April and persisted until about 0 UT on 14 April. Researchers at Gosan report that during this period the loading at the surface was so heavy that the yellow dust had to be cleaned from the car windshields before driving.

[38] Further corroboration of the different layering of dust and pollution aerosol comes from lidar depolarization observations performed in Nagasaki [*Shimizu et al.*, 2003], located east of the locations of the four Twin Otter vertical profiles discussed in this section (see map in Figure 1).

3.2. Water Vapor Closure

[39] In Figure 5 we compare 16 (of 26) vertical profiles of ρ_w obtained from AATS-14, and two T_d sensors aboard the Twin Otter: an EdgeTech 137-C3 chilled mirror and a Vaisala HMP 243 humidity sensor. In general, ρ_w from the two in situ sensors agrees very well, but the EdgeTech instrument is insensitive to $T_d < -35°C$, and the Vaisala sensor bottoms out at $T_d = -40°C$. This behavior of the EdgeTech sensor can be observed in Figures 5k and 5m.

[40] A comparison of ρ_w and layer water vapor LWV from all 26 vertical profiles is shown in the form of scatterplots in Figure 9. Although the correlation between AATS-14 and the two in situ sensors is high, AATS-14 systematically underestimates ρ_w and LWV, and leads to regression line slopes of 0.94 and 0.88, respectively. In light of the current controversy regarding H_2O spectroscopy in

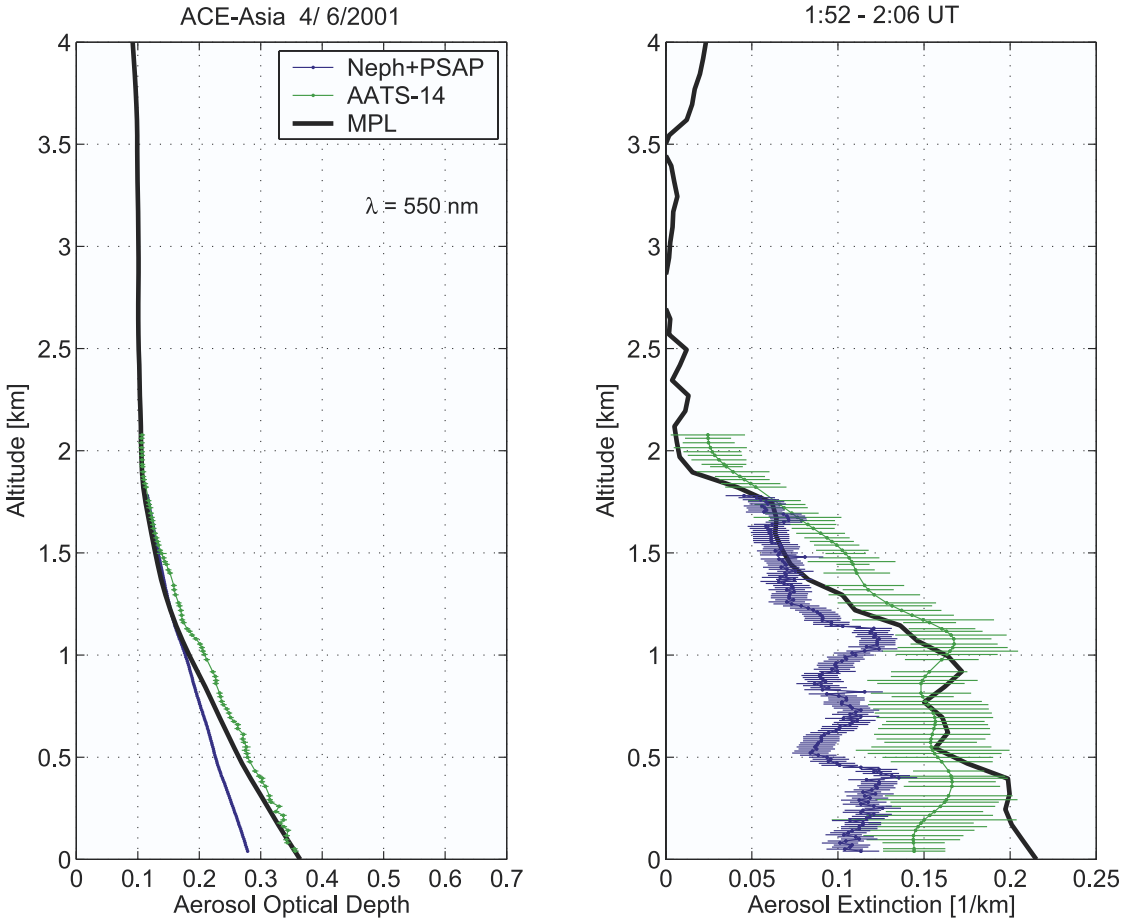

Figure 15. τ_p(550 nm) and σ_{ep}(550 nm) obtained from AATS-14 and the sum of scattering and absorption from Nephelometers and PSAP instruments and from MPL during a Twin Otter vertical profile over R/V *Ronald H. Brown* on 6 April 2001.

the near infrared [see, e.g., *Rothman et al.*, 2001; *Rothman and Schroeder*, 2002], which also entails discussion about the appropriateness of the H_2O CKD continuum used here [*Zhong et al.*, 2002], a disagreement at the level found here is not surprising. However, the corresponding water vapor closure study by *Redemann et al.* [2003] using AATS-6 and in situ data from the C-130 revealed no systematic difference. Since we are using the same method, spectroscopy, and continuum to derive water vapor for both AATS-6 and AATS-14, the ACE-Asia results seem to point to a discrepancy, which we are currently trying to resolve.

3.3. Aerosol Extinction Closure From AATS-14 and the Sum of in Situ Measured Scattering and Absorption

[41] A comparison of aerosol extinction $\sigma_{ep}(\lambda)$ vertical profiles from AATS-14 and the sum of scattering and absorption from nephelometers and PSAP instruments was possible for 14 ACE-Asia Twin Otter profiles. These 14 profiles are shown in Figure 10. To facilitate visual comparison with previous figures we used the same ordering of frames. The AATS-14 $\sigma_{ep}(\lambda)$ at 550 nm was interpolated using equation (7).

[42] A comparison of σ_{ep}(550 nm) and layer τ_p(550 nm) from the 14 vertical profiles is shown in the form of scatterplots in Figures 11 and 12. The σ_{ep}(550 nm) comparison yields 3663 data pairs covering a range of $0 \leq \sigma_{ep}(550\ \text{nm}) \leq \sim 0.3\ \text{km}^{-1}$. Since in such a comparison there are uncertainties in both variables (x and y) we used the least squares bi-sector method [*Sprent and Dolby*, 1980] to determine the regression line. This led to a slope of 0.873 (±0.003) and a small intercept of 0.003 (±0.001). The layer τ_p(550 nm) values shown in Figure 12 are computed by vertically integrating σ_{ep}(550 nm) over the altitude range where both AATS-14 and the in situ measurements are available. Error bars of $\tau_p(\lambda)$ for AATS-14 are based on horizontal distance spanned by a profile, combined with average horizontal variability of $\tau_p(\lambda)$ in ACE-Asia flights. Error bars of τ_p(550 nm) from Nephelometer and PSAP are based on instrument performance and uncertainties of corrections applied. Using the least squares bi-sector method to determine the regression line led to a slope of 0.747 (±0.096) and an intercept of 0.035 (±0.024). Inspection of Figure 12 reveals that the slope is heavily influenced by the disagreement found in the two cases with the largest τ_p(550 nm), corresponding to Figures 10f and 10h. We therefore believe that the slope of 0.873 (±0.003) found with the σ_{ep}(550 nm) comparison represent a better measure of the overall agreement.

[43] Further inspection of Figure 12 reveals that of the 14 cases, 6 show disagreement larger than the error bars. Of

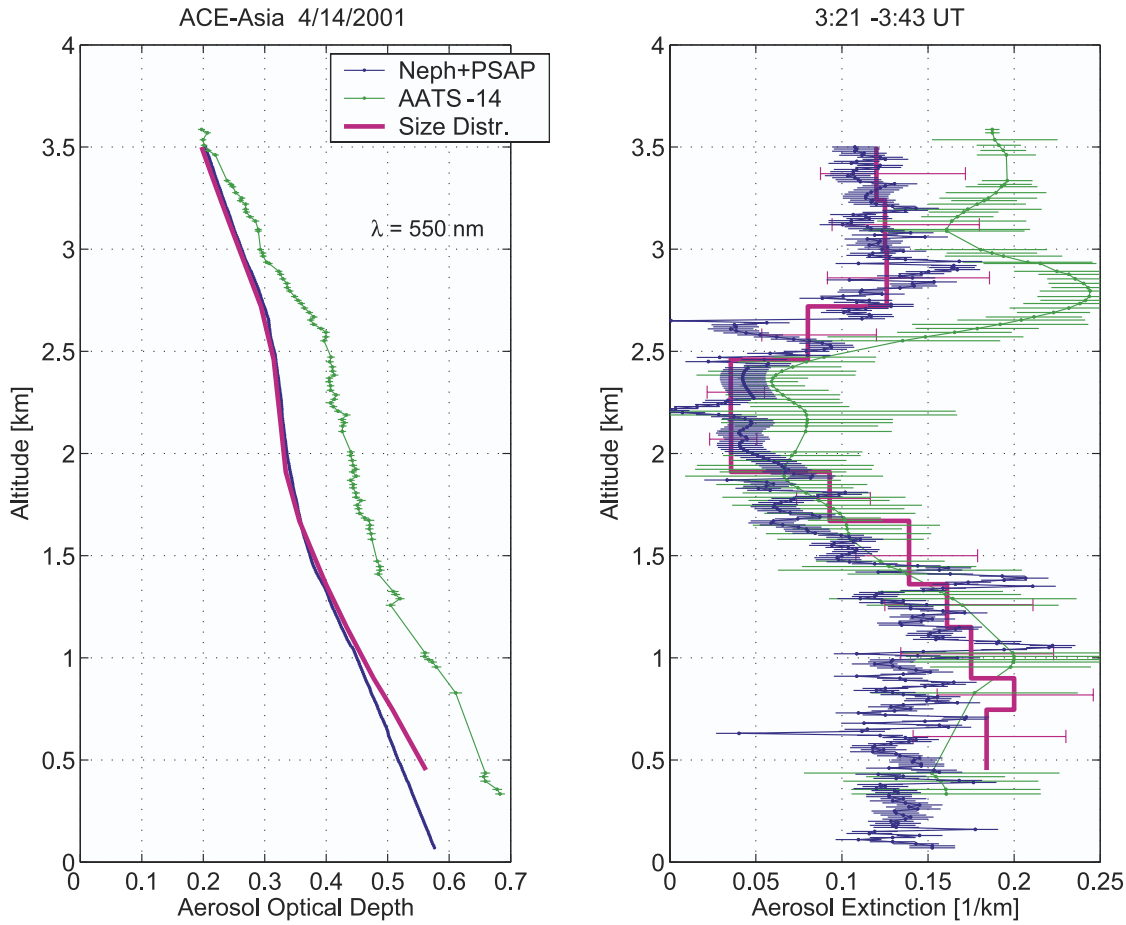

Figure 16. τ_p(550 nm) and σ_{ep}(550 nm) obtained from AATS-14, from the sum of scattering and absorption from Nephelometers and PSAP instruments and computed from size distributions during a Twin Otter vertical profile on 14 April 2001.

these 6, the in situ layer τ_p(550 nm) is smaller than the AATS-14 layer τ_p(550 nm) in four cases (corresponding to Figures 10b, 10c, 10f, and 10h) and larger in two cases (Figures 10g and 10o). It appears that the differences are not correlated with the presence of larger (dust) particles (identified with the spectral parameters in Figure 7), which could present added difficulties to the in situ measurement: While in Figure 10f the Neph+PSAP σ_{ep}(550 nm) are lower than the AATS-14 values in the elevated dust layer, the agreement is reasonable in the elevated dust layer in Figure 10h. The disagreement in Figure 10h is actually most pronounced in the pollution layer where the spectral parameters indicate small particles. Very similarly, we find disagreement in the MBL in Figures 10b and 10c, but only in one case (Figure 10c) is the MBL dominated by dust particles.

3.4. Comparison of Aerosol Extinction Profiles From AATS-14 and Ship-Based MPL

[44] On three occasions during ACE-Asia the Twin Otter flew a vertical profile at the ship's location. For these events we deviated somewhat from the standard MPLNET processing. The lidar data were first averaged over the time period it took the Twin Otter to complete the vertical profile. The lidar-derived σ_{ep}(523 nm) profile is then constrained by the total column τ_p(523 nm) and the τ_p(523 nm) at the top of the Twin Otter profile (both measured with AATS-14) with one lidar-ratio S_p(523 nm) from sea level to the top of the Twin Otter profile and one S_p(523 nm) for all altitudes above. Finally, we also computed implied S_p(523 nm) (as a function of altitude), representing the values that would be required to exactly reconcile the lidar return signal with the AATS14-measured extinction profile. We used the 525-nm AATS-14 channel with no adjustment for the small difference in wavelength. One Twin Otter/ship rendezvous was influenced by clouds and is thus not discussed here.

[45] The results for the rendezvous on 6 and 17 April 2001 are shown in Figures 13 and 14. Common to both cases is that aerosol with σ_{ep}(523 nm) < 0.050 km^{-1} (presumably dust) is detected at altitudes from 4 to 8 or even 10 km. Dust layers extending to similar altitudes were observed by lidars in Japan and instrumentation aboard the C-130 aircraft on 23 April 2001 [*Murayama et al.*, 2003; *Redemann et al.*, 2003; *Sakai et al.*, 2002].

[46] On 6 April the two-lidar-ratio approach yields S_p(523 nm) = 34.2 sr in the MBL sampled by the Twin Otter and S_a(523 nm) = 71 sr in the FT. The implied S_p(523 nm) increases from 23 to 55 sr with increasing altitude.

[47] On 17 April the two-lidar-ratio approach yields S_p(523 nm) = 37.5 sr in the altitude range sampled by the Twin Otter and S_p(523 nm) = 58.6 sr above The implied

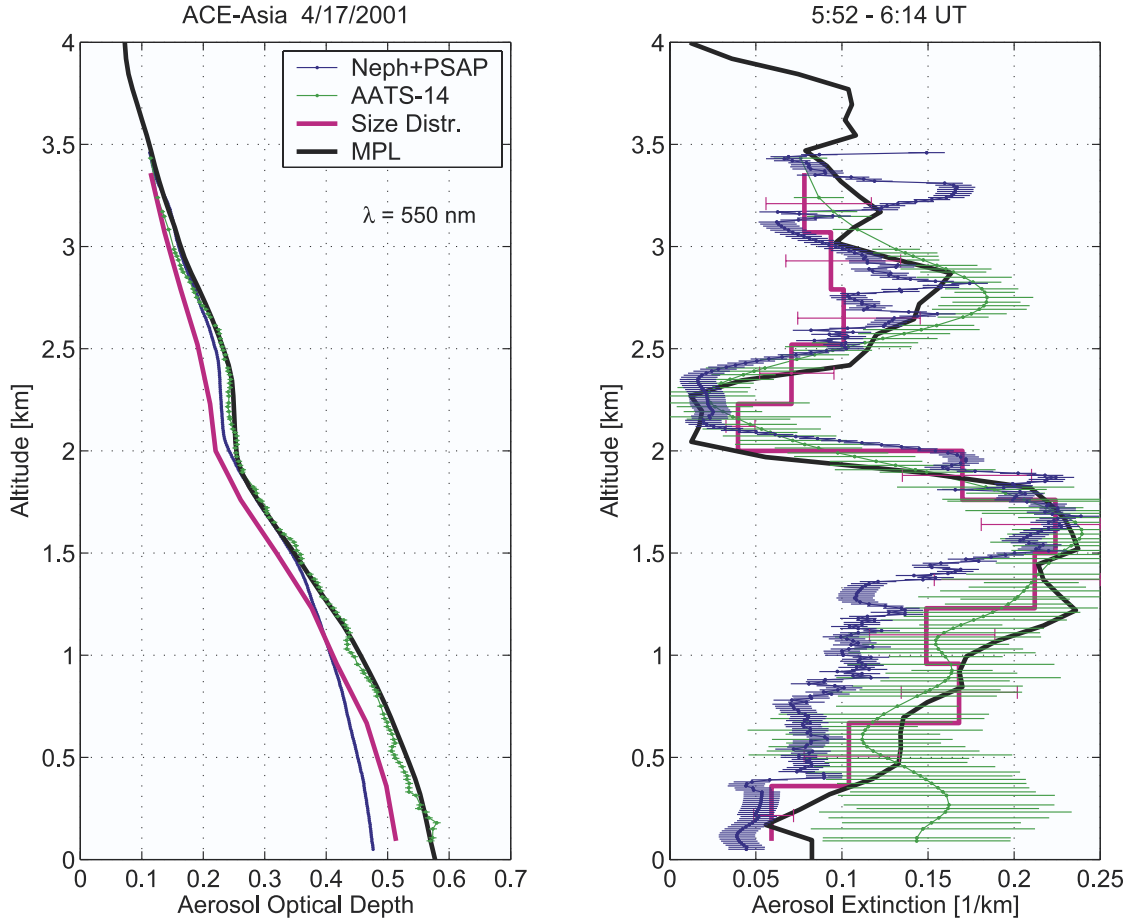

Figure 17. τ_p(550 nm) and σ_{ep}(550 nm) obtained from AATS-14, from the sum of scattering and absorption from Nephelometers and PSAP instruments, computed from size distributions and from ship-based MPL during a Twin Otter vertical profile over R/V *Ronald H. Brown* on 17 April 2001.

S_p(523 nm) varies slightly around the value obtained with the two-S_p-approach. The C-130 aircraft flew an ascent from near the surface to 5 km at the ship location two hours after the Twin Otter profile shown here. Combining data from an integrating Nephelometer, a PSAP, and a 180°-backscatter nephelometer [*Anderson et al.*, 2000, 2003] aboard the C-130 resulted in S_p(532 nm) ~45 sr throughout the profile (S. Masonis, personal communication, 2002). This value however, has not yet been corrected for the fact that the in situ measurements were performed at low relative humidity.

[48] *Murayama et al.* [2003] and *Sakai et al.* [2002] report S_p(532 nm) = 46.5 ± 10.5 sr and 46 ± 5 sr for an elevated dust layer (4–7 km) using Raman lidar night-time observations on 23 April with in situ measurements on the C-130 earlier in the day yielding 50.4 ± 9.4 sr (again at low RH).

[49] In a future publication we plan to compare our implied S_p(523 nm) with those computed from Twin Otter in situ size distributions [*Wang et al.*, 2002] and from size distributions inverted from AATS-14 $\sigma_{ep}(\lambda)$ spectra [*Kuzmanoski et al.*, 2002; *Schmid et al.*, 2000].

3.5. Aerosol Extinction Closure or Comparison From All Four Methods

[50] In the following we discuss five cases where profiles of $\tau_p(\lambda)$ and $\sigma_{ep}(\lambda)$ are available from at least three of the four methods discussed in this paper. All profiles are shown for λ = 550 nm. The MPL data have been adjusted to that wavelength using the wavelength dependence of $\sigma_{ep}(\lambda)$ found with AATS-14 (equation (7)).

[51] Figure 15 shows τ_p(550 nm) and σ_{ep}(550 nm) obtained from AATS-14, from the sum of scattering and absorption from Nephelometers and PSAP instruments, and from MPL during a Twin Otter vertical profile over the R/V *Ronald H. Brown* on 6 April 2001. The Nephelometer+PSAP τ_p(550 nm) profile is anchored to the AATS-14 τ_p(550 nm) at the top of the profile. The AATS-14 τ_p(550 nm) error bars are the measurement errors computed according to *Russell et al.* [1993a] and do not account for spatial variability. Error bars of σ_{ep}(550 nm) for AATS-14 are based on horizontal distance spanned by the profile, combined with average horizontal variability of $\tau_p(\lambda)$ in ACE-Asia flights. The MPL data is processed using the two lidar-ratio approach described earlier. As shown in Figure 13, a lidar ratio of 23 sr is needed to bring the MPL in agreement with AATS-14 near the surface. An even lower value would be needed to force agreement with the Nephelelometer+PSAP data.

[52] Figure 16 shows τ_p(550 nm) and σ_{ep}(550 nm) obtained from AATS-14, from the sum of scattering and absorption from Nephelometers and PSAP instruments and computed from size distributions during a vertical profile on 14 April 2001. The Nephelometer+PSAP σ_{ep}(550 nm) are

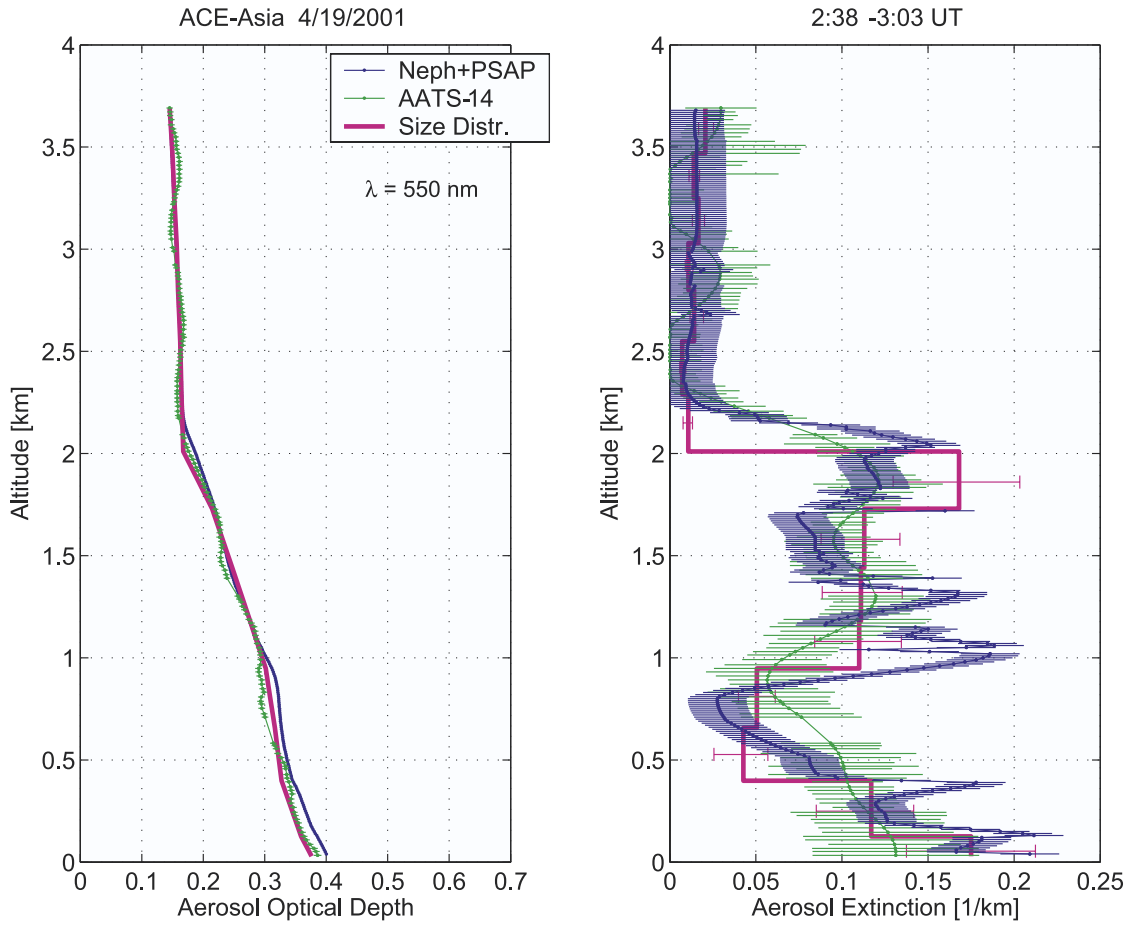

Figure 18. τ_p(550 nm) and σ_{ep}(550 nm) obtained from AATS-14, from the sum of scattering and absorption from Nephelometers and PSAP instruments and computed from size distributions during a Twin Otter vertical profile on 19 April 2001.

considerably lower in the elevated dust layer and in the MBL. σ_{ep}(550 nm) computed from size distributions follows the Nephelometer+PSAP curve in the dust but is closer to AATS-14 in the MBL.

[53] Figure 17 shows τ_p(550 nm) and σ_{ep}(550 nm) obtained from AATS-14, Nephelometer+PSAP, computed from size distributions, and from MPL during a Twin Otter vertical profile over the R/V *Ronald H. Brown* on 17 April 2001. Compared to AATS-14 the computed σ_{ep}(550 nm) is again significantly lower in the elevated dust layer but agrees well for most of the MBL. Nephelometer+PSAP σ_{ep}(550 nm) are slightly less than AATS-14 in the dust and significantly less in the MBL. The Nephelometer+PSAP also shows a layer near 3.3 km, which is not confirmed by the other three instruments.

[54] Figures 18 and 19 show τ_p(550 nm) and σ_{ep}(550 nm) obtained from AATS-14, and Nephelometer+PSAP data, and computed from size distributions for vertical profiles on 19 and 23 April 2001. In both cases there is good agreement among all three methods in terms of σ_{ep}(550 nm) and integrated τ_p(550 nm).

4. Summary and Conclusions

[55] We assess the consistency (closure) between solar beam attenuation by aerosols and water vapor measured by airborne Sun photometry and derived from airborne in situ, and ship-based lidar measurements during the ACE-Asia field experiment. The airborne data presented here were obtained aboard the Twin Otter aircraft. A companion paper [*Redemann et al.*, 2003] discusses closure results obtained from the C-130 aircraft.

[56] We have analyzed 26 lower tropospheric vertical profiles of $\tau_p(\lambda)$, CWV, $\sigma_{ep}(\lambda)$ and ρ_w obtained with AATS-14 over the ocean around Japan. A common feature is that often τ_p(499 nm) ~0.1 (total range 0.03–0.2) at ~3.5 km altitude revealing the prevalence of elevated dust layers. In fact, MPL retrievals from the ship (6 and 17 April) show dust layers extending to 10 km altitude. From the combined MPL/AATS-14 analysis we find the dust above 4 km to have S_p(523 nm) 59–71 sr, which is slightly higher than values found with Raman lidar and in situ measurements on a different day (23 April) [*Murayama et al.*, 2003; *Sakai et al.*, 2002].

[57] We find the spectral shape of $\sigma_{ep}(\lambda)$ to be a good indicator of particle size, with dust layers exhibiting an almost flat, slightly convexly curved spectrum.

[58] The Twin Otter water vapor results reveal a relatively dry atmosphere during ACE-Asia with all CWV < 1.5 cm and ρ_w < 12 g/m^3. The C-130 aircraft encountered similarly dry conditions with the exception of a flight on 30 April 2001 [*Redemann et al.*, 2003]. Comparing LWV and ρ_w from

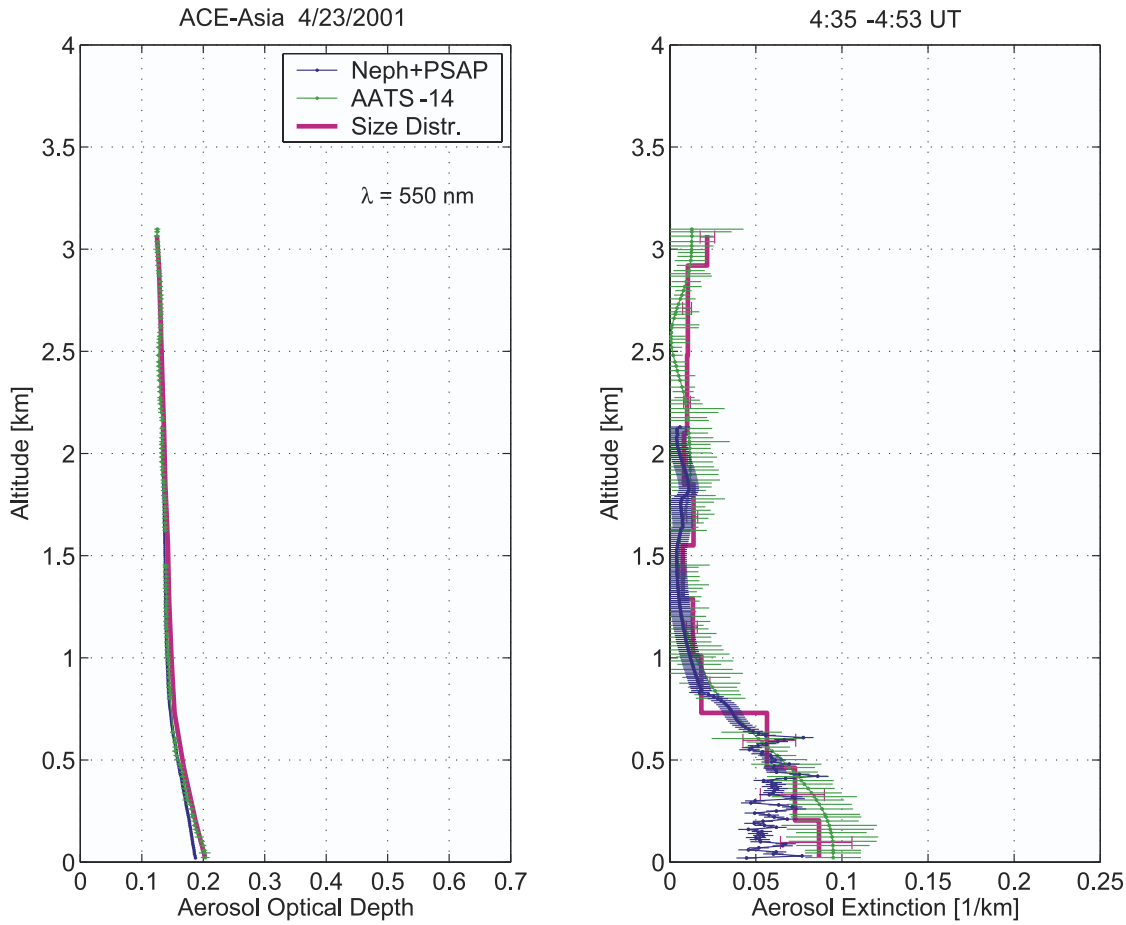

Figure 19. Same as Figure 18 but for a Twin Otter vertical profile on 23 April 2001.

AATS-14 to the same quantities measured with in situ sensors leads to a high correlation ($r^2 = 0.96$) but AATS-14 tends to underestimate ρ_w by 7%. The corresponding water vapor closure study using AATS-6 and in situ data from the C-130 revealed no systematic difference [*Redemann et al.*, 2003].

[59] Fourteen profiles of $\tau_p(\lambda)$ and $\sigma_{ep}(\lambda)$ were analyzed in terms of aerosol closure between AATS-14 and the sum of scattering and absorption from Nephelometers and PSAP instruments. When comparing layer $\tau_p(\lambda)$, 6 (of 14) cases show disagreement larger than the error bars. The comparison of $\sigma_{ep}(\lambda)$ reveals that the Nephelometers and PSAP results are ~13% lower than the AATS-14 results (based on slope of the least squares bisector line). We find no obvious correlation between the differences in $\sigma_{ep}(\lambda)$ and the size of the aerosols dominating the respective layers. The corresponding aerosol closure study using AATS-6 and Nephelometer+PSAP data from the C-130 led to slightly better agreement than found here [*Redemann et al.*, 2003]. The level of agreement found in this closure study and in TARFOX [*Hegg et al.*, 1997; *Hartley et al.*, 2000] is similar. Better agreement was found during SAFARI-2000 [*Magi et al.*, 2003], probably because the aerosol was dominated by small, spherical, relatively non-hygroscopic biomass burning particles and ambient RH was relatively low. The agreement found in ACE-2 was much poorer because the design of the aerosol inlet prevented the larger dust particles from being sampled. [*Schmid et al.*, 2000].

[60] Comparing σ_{ep}(550 nm) from the four different techniques shows good agreement for the vertical distribution of aerosol layers. However, the level of agreement in absolute magnitude of the derived aerosol extinction varied among the aerosol layers sampled. The σ_{ep}(550 nm) computed from size distribution and composition shows good agreement in the MBL but is considerably lower in layers dominated by dust. *Wang et al.* [2002] suggest that the discrepancy might be explained by the shape of the dust particles. They show that a nonspherical model of dust (doublet agglomerates) can produce agreement between predicted and observed extinction via the combined effect of larger APS-derived particle size and larger extinction-to-volume ratios. It is interesting to note that the *Wang et al.* [2002] study reproduces the shape of $\sigma_{ep}(\lambda = 354 - 1558$ nm) as measured by AATS-14, whereas the ACE-2 study of *Collins et al.* [2000] (using optical probes PCASP and FSSP instead of TDMA and APS used by *Wang et al.* [2002]) did not reproduce $\sigma_{ep}(\lambda > 1020$ nm) as measured by AATS-14.

[61] **Acknowledgments.** This research was conducted as part of the Asian Pacific Regional Aerosol Characterization Experiment (ACE-Asia). It is a contribution to the International Global Atmospheric Chemistry (IGAC) Core Project of the International Geosphere Biosphere Program (IGBP) and is part of the IGAC Aerosol Characterization Experiments (ACE). Funding to NASA Ames was provided by NASA's Earth Observing System Inter-Disciplinary Science (EOS-IDS) Program, NASA's Radiation Sciences Program, and the Office of Naval Research. Funding to the Department of Atmospheric Sciences, University of Washington, was provided by Office of Naval Research grant N00014-97-1-0132. We thank

the Ozone Processing Team at NASA Goddard Space Flight Center for making available TOMS EP data. We also would like to thank Edward T. Peltzer for making available Matlab shell-scripts for linear regression analysis (www.mbaeri.org/~etp3/regressindex.htm), and Atmospheric and Environmental Research Inc. (AER) for making LBLRTM available at http://www.rtweb.aer.com/.

References

Ackermann, J., The extinction-to-backscatter ratio of tropospheric aerosol: A numerical study, *J. Atmos. Oceanic Technol.*, *15*, 1043–1050, 1998.

Anderson, T. L., and J. A. Ogren, Determining aerosol radiative properties using the TSI 3563 integrating nephelometer, *Aerosol Sci. Technol.*, *29*, 57–69, 1998.

Anderson, T. L., S. J. Masonis, D. S. Covert, R. J. Charlson, and M. J. Rood, In situ measurement of the aerosol extinction-to-backscatter ratio at a polluted continental site, *J. Geophys. Res.*, *105*, 26,907–26,916, 2000.

Anderson, T. L., S. J. Masonis, D. S. Covert, N. A. Ahlquist, S. G. Howell, A. D. Clarke, and C. S. McNaughton, Variability of aerosol optical properties derived from in situ aircraft measurements during ACE-Asia, *J. Geophys. Res.*, *108*(D23), 8647, doi:10.1029/2002JD003247, in press, 2003.

Bluth, R. T., P. A. Durkee, J. H. Seinfeld, R. C. Flagan, L. M. Russell, P. A. Crowley, and P. Finn, Center for Interdisciplinary Remotely-Piloted Aircraft Studies (CIRPAS), *Bull. Am. Meteorol. Soc.*, *77*, 2691–2699, 1996.

Bögel, W., Neue Näherungsgleichungen für den Sättigungsdruck des Wasserdampfes und für die in der Meteorologie gebräuchlichen Luftfeuchte-Parameter, *DLR-FB 77–52*, Dtsch. Forsch.- und Versuchsanst. für Luft- und Raumfahrt, Oberpfaffenhofen, Germany, 1977.

Bond, T. C., T. L. Anderson, and D. Campbell, Calibration and intercomparison of filter-based measurements of visible light absorption by aerosols, *Aerosol Sci. Technol.*, *30*, 582–600, 1999.

Box, M. A., and A. Deepak, Atmospheric corrections to solar radiometry, *Appl. Opt.*, *18*, 1941–1949, 1979.

Clough, S. A., and M. J. Iacono, Line-by-line calculations of atmospheric fluxes and cooling rates: 2. Application to carbon dioxide, ozone, methane, nitrous oxide, and the halocarbons, *J. Geophys. Res.*, *100*, 16,519–16,535, 1995.

Collins, D. R., et al., In situ aerosol size distributions and clear column radiative closure during ACE-2, *Tellus, Ser. B*, *52*, 498–525, 2000.

Dubovik, O., B. Holben, T. F. Eck, A. Smirnov, Y. J. Kaufman, M. D. King, D. Tanré, and I. Slutsker, Variability of absorption and optical properties of key aerosol types observed in worldwide locations, *J. Atmos. Sci.*, *59*, 590–608, 2002.

Eck, T. F., B. N. Holben, J. S. Reid, O. Dubovik, A. Smirnov, N. T. O'Neill, I. Slutsker, and S. Kinne, Wavelength dependence of the optical depth of biomass burning, urban, and desert dust aerosols, *J. Geophys. Res.*, *104*, 31,333–31,349, 1999.

Fernald, F. G., Analysis of atmospheric lidar observations: Some comments, *Appl. Opt.*, *23*, 652–653, 1984.

Gao, S., D. A. Hegg, D. S. Covert, and H. Jonsson, Aerosol chemistry, and light-scattering and hygroscopicity budgets during outflow from east Asia, *Atmos. Chem*, in press, 2003.

Gassó, S., et al., Influence of humidity on the aerosol scattering coefficient and its effect on the upwelling radiance during ACE-2, *Tellus, Ser. B*, *52*, 546–567, 2000.

Harder, J. W., J. W. Brault, P. V. Johnston, and G. H. Mount, Temperature dependent NO_2 cross sections at high spectral resolution, *J. Geophys. Res.*, *102*, 3861–3879, 1997.

Hartley, W. S., P. V. Hobbs, J. L. Ross, P. B. Russell, and J. M. Livingston, Properties of aerosols aloft relevant to direct radiative forcing off the mid-Atlantic coast of the United States, *J. Geophys. Res.*, *105*, 9859–9886, 2000.

Hegg, D. A., J. Livingston, P. V. Hobbs, T. Novakov, and P. Russell, Chemical apportionment of aerosol column optical depth off the mid-Atlantic coast of the United States, *J. Geophys. Res.*, *102*, 25,293–25,303, 1997.

Holben, B. N., et al., AERONET: A Federated Instrument Network and Data Archive for Aerosol Characterization, *Remote Sens. Environ.*, *66*, 1–16, 1998.

Huebert, B. J., T. Bates, P. B. Russell, G. Shi, Y. J. Kim, K. Kawamura, G. Carmichael, and T. Nakajima, An overview of ACE-Asia: Strategies for quantifying the relationships between Asian aerosols and their climatic impacts, *J. Geophys. Res.*, *108*(D23), 8633, doi:10.1029/2003JD003550, in press, 2003.

Kasten, F., Visibility in the phase of pre-condensation, *Tellus*, *21*, 631–635, 1969.

Kaufman, Y. J., D. Tanré, and O. Boucher, A satellite view of aerosols in the climate system, *Nature*, *419*, 215–223, 1996.

King, M. D., and D. M. Byrne, A method for inferring total ozone content from the spectral variation of total optical depth obtained with a solar radiometer, *J. Atmos. Sci.*, *33*, 2242–2251, 1976.

Kinne, S., T. P. Ackerman, M. Shiobara, A. Uchiyama, A. J. Heymsfield, L. Milosevich, J. Wendell, E. W. Eloranta, C. Purgold, and R. W. Bergstrom, Cirrus cloud radiative and microphysical properties from ground observations and in situ measurements during FIRE 1991 and their application to exhibit problems in cirrus solar radiative transfer modeling, *J. Atmos. Sci.*, *54*, 2320–2344, 1997.

Kuzmanoski, M., M. Box, G. P. Box, B. Schmid, P. B. Russell, J. Redemann, J. M. Livingston, J. Wang, R. C. Flagan, and J. H. Seinfeld, Aerosol size distributions during ACE-Asia: Retrievals from optical thickness and comparisons with in-situ measurements, *Eos Trans. AGU*, *83*(47), Fall Meet. Suppl., F128, 2002.

Livingston, J. M., et al., Airborne Sun photometer measurements of aerosol optical depth and columnar water vapor during the Puerto Rico Dust Experiment and comparison with land, aircraft, and satellite measurements, *J. Geophys. Res.*, *108*(D19), 8588, doi:10.1029/2002JD002520, 2003.

Magi, B. I., P. V. Hobbs, B. Schmid, and J. Redemann, Vertical profiles of light scattering, light absorption, and single scattering albedo during the dry, biomass burning season in southern Africa and comparisons of in situ and remote sensing measurements of aerosol optical depths, *J. Geophys. Res.*, *108*(D13), 8504, doi:10.1029/2002JD002361, 2003.

Masonis, S. J., K. Franke, A. Ansmann, D. Müller, D. Althausen, J. A. Ogren, A. Jefferson, and P. J. Sheridan, An intercomparison of aerosol light extinction and 180° backscatter as derived using in situ instruments and Raman lidar during the INDOEX field campaign, *J. Geophys. Res.*, *107*(D19), 8014, doi:10.1029/2000JD000035, 2002.

Matsumoto, T., P. B. Russell, C. Mina, W. Van Ark, and V. Banta, Airborne Tracking Sunphotometer, *J. Atmos. Oceanic Technol.*, *4*, 336–339, 1987.

Michalsky, J. J., J. C. Liljegren, and L. C. Harrison, A comparison of Sun photometer derivations of total column water vapor and ozone to standard measures of same at the Southern Great Plains Atmospheric Radiation Measurement site, *J. Geophys. Res.*, *100*, 25,995–26,003, 1995.

Murayama, T., et al., An intercomparison of lidar-derived aerosol optical properties with airborne measurements near Tokyo during ACE-Asia, *J. Geophys. Res.*, *108*(D23), 8651, doi:10.1029/2002JD003259, in press, 2003.

Ramanathan, V., P. J. Crutzen, J. T. Kiehl, and D. Rosenfeld, Aerosol, climate and the hydrological cycle, *Science*, *294*, 2119–2124, 2001.

Redemann, J., P. B. Russell, and P. Hamill, Dependence of aerosol light absorption and single-scattering albedo on ambient relative humidity for sulfate aerosols with black carbon cores, *J. Geophys. Res.*, *106*, 27,485–27,495, 2001.

Redemann, J., S. Masonis, B. Schmid, T. Anderson, P. Russell, J. Livingston, O. Dubovik, and A. Clarke, Clear-column closure studies of aerosols and water vapor aboard the NCAR C-130 in ACE-Asia, 2001, *J. Geophys. Res.*, *108*(D23), 8655, doi:10.1029/2003JD003442, in press, 2003.

Rothman, L. S., and J. Schroeder, Millenium HITRAN compilation, paper presented at 12th ARM Science Team Meeting, ARM Program, St. Petersburg, Fla., 8 –12 April 2002.

Rothman, L. S., K. Chance, J. Schroeder, and A. Goldman, New edition of HITRAN database, paper presented at 11th ARM Science Team Meeting, ARM Program, Atlanta, Ga., 19 –23 March 2001.

Russell, P. B., et al., Pinatubo and pre-Pinatubo optical-depth spectra: Mauna Loa measurements, comparisons, inferred particle size distributions, radiative effects, and relationship to lidar data, *J. Geophys. Res.*, *98*, 22,969–22,985, 1993a.

Russell, P. B., et al., Post-Pinatubo optical depth spectra vs. latitude and vortex structure: Airborne Tracking Sunphotometer measurements in AASE II, *Geophys. Res. Lett.*, *20*, 2571–2574, 1993b.

Russell, P. B., P. V. Hobbs, and L. L. Stowe, Aerosol properties and radiative effects in the United States Mid-Atlantic haze plume: An overview of the Tropospheric Aerosol Radiative Forcing Observational Experiment (TARFOX), *J. Geophys. Res.*, *104*, 2213–2222, 1999a.

Russell, P. B., J. M. Livingston, P. Hignett, S. Kinne, J. Wong, and P. V. Hobbs, Aerosol-induced radiative flux changes off the United States Mid-Atlantic coast, Comparison of values calculated from Sun photometer and in situ data with those measured by airborne pyranometer, *J. Geophys. Res.*, *104*, 2289–2307, 1999b.

Sakai, T., et al., Case study of Raman lidar measurements of Asian dust events in 2000 and 2001 at Nagoya and Tsukuba, Japan, *Atmos. Environ.*, *36*, 5479–5489, 2002.

Schmid, B., and C. Wehrli, Comparison of sun photometer calibration by Langley technique and standard lamp, *Appl. Opt.*, *34*, 4500–4512, 1995.

Schmid, B., K. J. Thome, P. Demoulin, R. Peter, and J. Sekler, Comparison of modeled and empirical approaches for retrieving columnar water vapor

from solar transmittance measurements in the 0. 94 micron region, *J. Geophys. Res.*, *101*, 9345–9358, 1996.

Schmid, B., C. Mätzler, A. Heimo, and N. Kämpfer, Retrieval of optical depth and size distribution of tropospheric and stratospheric aerosols by means of sun photometry, *IEEE Trans. Geosci. Remote Sens.*, *35*, 172–182, 1997.

Schmid, B., P. R. Spyak, S. F. Biggar, C. Wehrli, J. Sekler, T. Ingold, C. Mätzler, and N. Kämpfer, Evaluation of the applicability of solar and lamp radiometric calibrations of a precision Sun photometer operating between 300 and 1025 nm, *Appl. Opt.*, *37*, 3923–3941, 1998.

Schmid, B., et al., Clear sky closure studies of lower tropospheric aerosol and water vapor during ACE 2 using airborne Sun photometer, airborne in-situ, space-borne, and ground-based measurements, *Tellus, Ser. B*, *52*, 568–593, 2000.

Schmid, B., et al., Comparison of columnar water-vapor measurements from solar transmittance methods, *Appl. Opt.*, *40*, 1886–1896, 2001.

Schmid, B., et al., Coordinated airborne, spaceborne, and ground-based measurements of massive, thick aerosol layers during the dry season in southern Africa, *J. Geophys. Res*, *108*(D13), 8496, doi:10.1029/2002JD002297, 2003.

Shimizu, A., N. Sugimoto, I. Matsui, K. Arao, I. Uno, T. Murayama, N. Kagawa, K. Aoki, A. Uchiyama, and A. Yamazaki, Continuous observations of Asian dust and other aerosols by polarization lidars in China and Japan during ACE-Asia, *J. Geophys. Res.*, *108*, doi:10.1029/2002JD003253, in press, 2003.

Shiobara, M., and S. Asano, Estimation of cirrus optical thickness from Sun photometer measurements, *J. Appl. Meteorol.*, *33*, 672–681, 1994.

Spinhirne, J. D., J. A. R. Rall, and V. S. Scott, Compact eye safe lidar systems, *Rev. Laser Eng.*, *23*, 112–118, 1995.

Sprent, P., and G. Dolby, The geometric mean functional relationship, *Biometrics*, *36*, 547–550, 1980.

Wang, J., et al., Clear-column radiative closure during ACE-Asia: Comparison of multiwavelength extinction derived from particle size and composition with results from Sun photometry, *J. Geophys. Res.*, *107*(D23), 4688, doi:10.1029/2002JD002465, 2002.

Welton, E. J., J. R. Campbell, J. D. Spinhirne, and V. S. Scott, Global monitoring of clouds and aerosols using a network of micro-pulse lidar systems, in *Lidar Remote Sensing for Industry and Environmental Monitoring*, edited by U. N. Singh, T. Itabe, and N. Sugimoto, *Proc. SPIE Int. Soc. Opt. Eng.*, *4153*, 151–158, 2001.

Zhong, W., J. D. Haigh, D. Belmiloud, R. Schermaul, and J. Tennyson, Note on 'The impact of new water vapour spectral line parameters on the calculation of atmospheric absorption' by Weyi Zhong et al. (July A, 2001, 127, 1615–1626), *Q. J. R. Meteorol. Soc.*, *128*, 1387–1388, 2002.

D. Bates, Physics Department, University of Miami, 1320 Campo Sano Drive, Coral Gables, FL 33146, USA. (bates@physics.miami.edu)

D. S. Covert and D. A. Hegg, Department of Atmospheric Sciences, University of Washington, Box 351640, Seattle, WA 98195-1640, USA. (dcovert@u.washington.edu; deanhegg@atmos.washington.edu)

O. Dubovik, Goddard Earth Sciences and Technology Center, NASA Goddard Space Flight Center, Code 912, Greenbelt, MD 20771, USA. (dubovik@aeronet.gsfc.nasa.gov)

R. C. Flagan and J. H. Seinfeld, California Institute of Technology, 1200 E. California Blvd., Pasadena, CA 91125, USA. (flagan@cheme.caltech.edu; seinfeld@caltech.edu)

A. Jefferson, Cooperative Institute for Research in the Environmental Sciences, NOAA Climate Monitoring and Diagnostics Laboratory, Boulder, CO 80803, USA. (anne.jefferson@noaa.gov)

H. H. Jonsson, CIRPAS, 3240 Imjin Road, Marina, CA 93933, USA. (hjonsson@nps.navy.mil)

J. M. Livingston, J. Redemann, P. B. Russell, and B. Schmid, NASA Ames Research Center, MS 245-5, Moffett Field, CA 94035-1000, USA. (jlivingston@mail.arc.nasa.gov; jredemann@mail.arc.nasa.gov; bschmid@mail.arc.nasa.gov; philip.b.russell@nasa.gov)

J. Wang, Brookhaven National Laboratory, Upton, NY 11973, USA. (jian@bnl.gov)

E. J. Welton, Laboratory for Atmospheres, NASA Goddard Space Flight Center, Code 912, Greenbelt, MD 20771, USA. (ellsworth.j.welton@nasa.gov)